ELECTROCHEMISTRY

10.1126/sciadv.1501554

A universal cooperative assembly-directed method for coating of mesoporous TiO_2 nanoshells with enhanced lithium storage properties

Bu Yuan Guan,[1] Le Yu,[1] Ju Li,[2]* Xiong Wen (David) Lou[1]*

TiO_2 is exceptionally useful, but it remains a great challenge to develop a universal method to coat TiO_2 nanoshells on different functional materials. We report a one-pot, low-temperature, and facile method that can rapidly form mesoporous TiO_2 shells on various inorganic, organic, and inorganic-organic composite materials, including silica-based, metal, metal oxide, organic polymer, carbon-based, and metal-organic framework nanomaterials via a cooperative assembly-directed strategy. In constructing hollow, core-shell, and yolk-shell geometries, both amorphous and crystalline TiO_2 nanoshells are demonstrated with excellent control. When used as electrode materials for lithium ion batteries, these crystalline TiO_2 nanoshells composed of very small nanocrystals exhibit remarkably long-term cycling stability over 1000 cycles. The electrochemical properties demonstrate that these TiO_2 nanoshells are promising anode materials.

INTRODUCTION

Titanium dioxide (TiO_2) is probably the most studied metal oxide due to low cost, low toxicity, high thermal and chemical stabilities, and excellent optical and electronic properties (*1*). These favorable features render TiO_2 materials very attractive for sensing (*2*), catalysis (*3*–*6*), solar energy conversion (*7*–*9*), energy storage (*10*–*13*), and many other applications (*14*). To enrich the architecture and functionalities of nanomaterials, numerous methods have been developed to synthesize core@TiO_2 particles and their derived hollow nanostructures. Among the strategies for forming TiO_2 shells on materials, the sol-gel coating approach has often been used (*15*–*23*). However, unlike silica (SiO_2), it is very difficult to precisely control the sol-gel chemistry and crystallinity of TiO_2 on substrate surface. For example, a general method similar to the Stöber process for silica has been developed to synthesize porous TiO_2 shells for making multifunctional core-shell particles (*24*). To control the crystallization process of TiO_2 shells, a multistep "silica-protected calcination" strategy has been developed to synthesize high-quality TiO_2 hollow spheres with controlled nanosized TiO_2 grains in the shells (*25*). In our experience, the methods above still require delicate controls of the synthesis conditions. Meanwhile, the atomic layer deposition (ALD) method can deposit titania layers with a precisely (<1 nm) controlled thickness (*26*, *27*). However, the ALD method is relatively time-consuming. In addition, it requires expensive ALD instruments, which increase the cost and hamper large-scale production. A universal recipe for the facile coating of mesoporous TiO_2 shells on functional nanomaterials at room temperature is not known. Therefore, it is highly desirable and technically very important to develop a universal method for synthesizing TiO_2-enhanced nanocomposites for a diverse range of applications.

According to the hydrolysis polymerization reaction mechanism, TiO_2 has similar sol-gel reaction as SiO_2 (*28*, *29*). In addition, TiO_2 precursors [for example, titanium isopropoxide (TIP)] also have similar molecular structures to commonly used SiO_2 precursors [for example, tetraethyl orthosilicate (TEOS)], and both TIP and TEOS can form three-dimensional -O-M-O-M-O- networks through the sol-gel process. Both TiO_2 and SiO_2 aerogels have been synthesized via the sol-gel process by using an acid or base catalyst (*29*). In the presence of ammonia as a catalyst, core@TiO_2 (*24*) and core@SiO_2 (*30*) nanospheres are synthesized by the Stöber process. Also, an inorganic-organic self-assembly method has been developed to synthesize ordered mesoporous TiO_2 (*31*), which is analogous to the synthesis of mesoporous SiO_2 by using triblock polymers as soft templates (*32*, *33*).

The cooperative assembly-directed strategy has been widely used for the general coating of various functional materials with mesoporous SiO_2 shells (*34*–*38*). The synthesis usually involves self-assembled soft core particles, structure-directing agents [for example, cetyltrimethylammonium bromide (CTAB)], and SiO_2 precursors (for example, TEOS) in a water/ethanol mixture solution under alkaline conditions (for example, ammonia). By using this method, it is very easy to control the thickness (*35*), pore structure (*39*), and functionality (*40*) of the silica shells. However, this cooperative assembly-directed strategy rarely works for other materials (*41*).

Among its various potential applications, TiO_2 has been extensively studied as a promising anode material for lithium ion batteries (LIBs) (*12*, *42*). It has been demonstrated that nanoshells with well-defined hollow cavity can stabilize the nanoparticles against agglomeration and keep electrically connected to other grains, leading to superior cycling performance (*43*, *44*). Hence, enhanced lithium storage properties are generally expected from mesoporous TiO_2 nanoshells.

Here, we develop a universal method for growing mesostructured TiO_2 shells on diverse functional particles through a cooperative assembly-directed process at room temperature within 10 min. As a first demonstration, we show that high-quality TiO_2 hollow or yolk-shell spheres with tunable cavity size and shell thickness can be easily generated by alkaline etching of SiO_2 cores in SiO_2@TiO_2 or SiO_2 interlayers in core@SiO_2@TiO_2 particles. We further show that high-quality amorphous and crystalline mesoporous TiO_2 shells can also be grown on diverse functional particles, including metal and metal-oxide nanoparticles, mesoporous silica nanoparticles (MSNs), polymer

[1]School of Chemical and Biomedical Engineering, Nanyang Technological University, 62 Nanyang Drive, Singapore 637459, Singapore. [2]Department of Nuclear Science and Engineering and Department of Materials Science and Engineering, Massachusetts Institute of Technology, Cambridge, MA 02139, USA.
*Corresponding author. E-mail: liju@mit.edu (J.L.); xwlou@ntu.edu.sg (X.W.L.)

nanospheres (PNs), graphene oxide (GO), carbon nanospheres (CNs), and metal-organic framework (MOF) nanocrystals. Last, we demonstrate the potential use of these mesoporous TiO_2 nanoshells as anode materials for LIBs with long-term cycling stability.

RESULTS

The general synthesis procedure is very simple and illustrated in Fig. 1. The nanoparticles to be coated are homogeneously dispersed in ethanol by ultrasonication, followed by the addition of hexadecylamine (HDA) surfactants and ammonia under stirring. The HDA surfactants segregate to the surface of the nanoparticles. Then, TIP is added to the dispersion under stirring. The amino groups of the HDA molecules participate in hydrogen-bonding interactions with a TIP hydrolysis product (TiO_2) to form inorganic-organic composites that coat the nanoparticle, whereas the hydrophobic long carbon chains of HDA self-organize into rodlike micelles that will become pores in TiO_2 domains. This process generally completes at room temperature within 10 min. To remove the organic species, we perform a follow-up solvothermal treatment at 160°C. Depending on whether ammonia is used during the treatment, either amorphous TiO_2 ($a$$TiO_2$) or crystalline TiO_2 ($c$$TiO_2$) will remain as the nanoshell.

Synthesis of mesoporous $a$$TiO_2$ shells

In a typical synthesis, SiO_2 nanospheres with an average diameter of 220 nm (Fig. 2A and fig. S1A) are used as the core, and HDA is used as the surfactant for the formation of TiO_2 mesostructures. Figure 2B shows a transmission electron microscopy (TEM) image of the formed SiO_2@TiO_2/HDA core-shell spheres with a total diameter of 340 nm and shell thickness of 60 nm. The core-shell spheres are nearly monodisperse, and the surfaces are very smooth (fig. S1B). These SiO_2@TiO_2/HDA core-shell spheres are transformed into SiO_2@$a$$TiO_2$ yolk-shell nanospheres (Fig. 2, C and D) through a solvothermal treatment at 160°C in ammonia solution (0.5 M) for 16 hours. Each SiO_2@$a$$TiO_2$ yolk-shell nanosphere contains a small SiO_2 core with a diameter of about 70 nm, hollow cavity, and a uniform TiO_2 shell with a thickness of about 60 nm. The yolk-shell spheres obtained are still smooth and uniform without any cracks in the shells, in agreement with the field-emission scanning electron microscopy (FESEM) observation (fig. S1C).

To further characterize the uniform TiO_2 coating on the SiO_2 nanospheres, we characterize the hydrodynamic diameters of SiO_2 and SiO_2@TiO_2/HDA nanospheres with dynamic light scattering (DLS). The distributions in both DLS curves (fig. S2) are quite similar, with polydispersity index of only about 1%. The hydrodynamic diameter of SiO_2@TiO_2/HDA nanospheres is larger than that of SiO_2 nanospheres by about 130 nm. The cooperative self-assembly of TiO_2 and HDA is evidenced by small-angle x-ray diffraction (XRD) analysis (fig. S3). The XRD pattern of SiO_2@TiO_2/HDA nanospheres shows one broad diffraction peak at about 2.0°, suggesting the formation of mesostructured TiO_2 shells. The status of the HDA molecules before solvothermal treatment is probed by Fourier transform infrared (FTIR) analysis (fig. S4). The bands of $-NH_2$ stretching vibration near 3340 cm^{-1} and N–H wagging vibration at 810 cm^{-1} disappear, and the band of N–H deformation vibration shifts from 1570 to 1510 cm^{-1}. This indicates the strong interaction between HDA and TiO_2 in the mesostructured TiO_2 shell. The wide-angle XRD patterns (fig. S5) confirm the amorphous nature of the obtained SiO_2@TiO_2/HDA core-shell nanospheres. After the solvothermal treatment under alkaline condition, the obtained yolk-shell particles (SiO_2@$a$$TiO_2$) are still amorphous. The Brunauer-Emmett-Teller (BET) specific surface area of the SiO_2@TiO_2/HDA core-shell nanospheres is very small (S_{BET} < 10 m^2 g^{-1}) (fig. S6A). After the solvothermal treatment under alkaline condition, the HDA molecules are mostly removed (fig. S7) to generate mesopores with the diameter in the range from 2 to 3 nm (fig. S6B), which gives rise to a drastically increased BET surface area of 329 m^2 g^{-1}.

Hollow TiO_2 nanospheres with an amorphous shell can be obtained by the solvothermal treatment of SiO_2@TiO_2/HDA core-shell nanospheres at 160°C in ammonia solution (0.5 M) for 24 hours (fig. S8, A and B), which etches away the SiO_2 core completely. Compared with SiO_2@$a$$TiO_2$ yolk-shell spheres, the BET surface area of $a$$TiO_2$ hollow spheres increases to 342 m^2 g^{-1} (fig. S9). The diameter, interior cavity size, and shell thickness of mesoporous TiO_2 hollow spheres can be precisely tailored at the nanoscale by tuning the amount of Ti precursor and the particle size of SiO_2 template nanospheres. The as-prepared TiO_2 hollow spheres are highly uniform with smooth surfaces (fig. S10). As shown in Fig. 3, the shell thickness can be easily varied

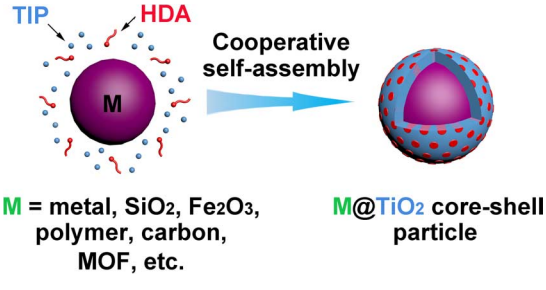

Fig. 1. Schematic illustration of the synthesis procedure for mesostructured TiO_2 shells.

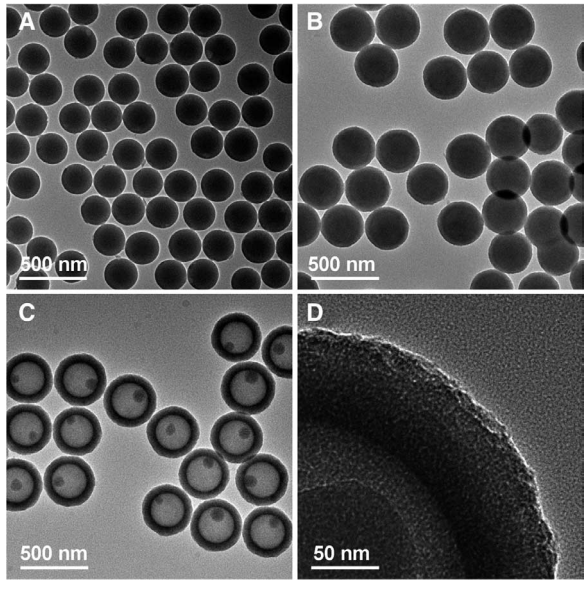

Fig. 2. TEM characterizations of SiO_2@TiO_2/HDA core-shell spheres and SiO_2@$a$$TiO_2$ yolk-shell spheres. (**A**) SiO_2 template spheres. (**B**) SiO_2@TiO_2/HDA core-shell spheres. (**C** and **D**) SiO_2@$a$$TiO_2$ yolk-shell spheres.

from 8 to 54 nm, and the cavity size is tuned in the range from 270 to 475 nm.

Synthesis of mesoporous TiO_2 shells with nanosized crystalline domains

SiO_2@*c*TiO_2 core-shell nanospheres with a crystalline shell are obtained via a solvothermal treatment at 160°C without the addition of ammonia (fig. S11A). The HDA molecules are mostly removed to generate mesopores with the size in the range from 5 to 6 nm, which gives rise to a BET surface area of 186 $m^2 g^{-1}$ (fig. S12). The *a*TiO_2 in the precursor is transformed to anatase phase (fig. S13). The different degrees of crystallinity between the TiO_2 samples obtained under alkaline and neutral conditions might be due to the suppressing effect of silica on the crystallization process. Similar phenomena have also been observed in other SiO_2/TiO_2 reaction systems (*25*, *45*). After the calcination in air (fig. S11B) and removal of silica template spheres, the *c*TiO_2 hollow spheres retain their morphology without apparent damage (Fig. 4, A and B). As can be seen from the rough surface of the nanosphere in the TEM image (Fig. 4C), the *c*TiO_2 nanoshell is composed of very small nanoparticles (~12 nm). At a high magnification, disordered intercrystallite mesopores and very small nanocrystals are clearly observed within the shell (Fig. 4D). A high-resolution TEM (HRTEM) image reveals lattice fringes of the nanocrystals, which can be correlated to the (101) planes of anatase TiO_2 (Fig. 4E). The distinct selected area electron diffraction (SAED) pattern also confirms the anatase phase of the sample (Fig. 4F). The BET surface

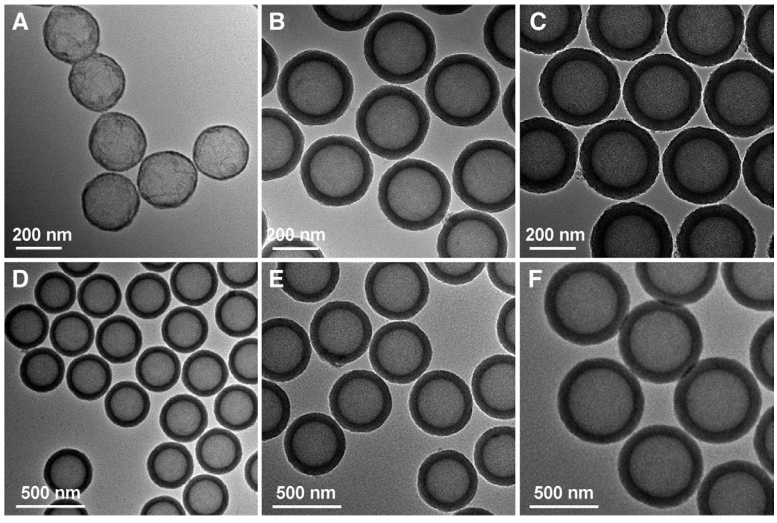

Fig. 3. TEM characterizations of mesoporous *a*TiO_2 hollow spheres. (**A** to **C**) *a*TiO_2 hollow spheres with identical hollow core size of about 230 nm but varied shell thicknesses: 8 nm (A), 41 nm (B), and 54 nm (C). (**D** to **F**) *a*TiO_2 hollow spheres with average diameter (core size) of 300 (270) nm (D), 410 (325) nm (E), and 680 (475) nm (F).

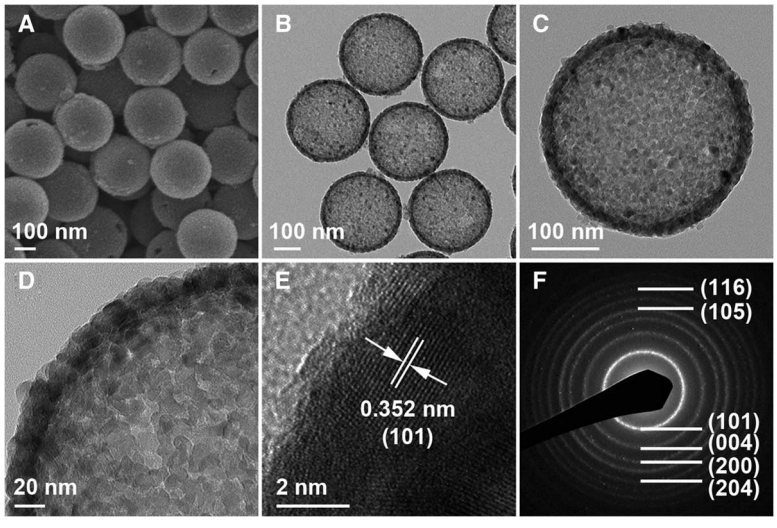

Fig. 4. FESEM and TEM characterizations of mesoporous *c*TiO_2 hollow spheres. (**A** and **B**) FESEM (A) and TEM images (B) of *c*TiO_2 hollow nanospheres. (**C** and **D**) Magnified TEM images show an individual *c*TiO_2 hollow nanosphere (C) and the mesoporous shell (D). (**E**) HRTEM image of the *c*TiO_2 shell. (**F**) Corresponding SAED pattern of *c*TiO_2 hollow nanospheres.

area of cTiO$_2$ hollow spheres is 176 m^2 g^{-1} (fig. S14) and is comparable to many other reported porous TiO$_2$ hollow particles (*15*, *24*, *25*, *45*). No peaks corresponding to Si element are found in the energy-dispersive x-ray spectroscopy spectrum (fig. S15), indicating the purity of the cTiO$_2$ nanoshells. Moreover, the pH value has some effect on the structure and crystallinity of the final products during the solvothermal process (fig. S16).

Yolk-shell and core-shell particles with various functional core materials

In addition to TiO$_2$ hollow spheres, yolk-shell particles with mesoporous TiO$_2$ shells can be easily prepared. It is very easy to coat a layer of silica on different materials to form core-shell structures. After that, a TiO$_2$ shell can be further grown on the core-shell particles to generate three-layered core@SiO$_2$@TiO$_2$ structures. As a demonstration, two such structures are prepared with Au nanoparticles and Fe$_2$O$_3$ cubes as the inner cores. After selectively etching the SiO$_2$ interlayer, Au@TiO$_2$ yolk-shell nanospheres and Fe$_2$O$_3$@TiO$_2$ yolk-shell cubes can be obtained under alkaline conditions (Fig. 5, A and B, and figs. S17 and S18). A double-shell TiO$_2$-polymer hollow structure with two functional materials in the shell can also be obtained by coating a polymer layer on the hollow TiO$_2$ spheres (Fig. 5C and fig. S19).

We further demonstrate the versatility of our method by growing a layer of mesostructured TiO$_2$ on many other commonly used materials, including MSNs, PNs, GO, CNs, and MOF nanocrystals (Fig. 5, D to H, and figs. S20 to S22). This versatile method could even be applied to form mesostructured TiO$_2$ layers on HNO$_3$-treated hydrophilic carbon nanotubes (CNTs) with many functional groups and untreated hydrophobic CNTs to synthesize smaller core-shell structures with a diameter of about 50 nm (fig. S23). Magnified TEM images and small-angle XRD patterns of representative samples further confirm the formation of mesostructured TiO$_2$ shells on diverse materials (fig. S24). These results indicate that the formation of a mesostructured TiO$_2$ layer by this assembly-directed method is facile and universal, independent of composition, surface functional groups, hydrophilicity, curvature, and size of the substrate particles.

Electrochemical performance for lithium storage

To demonstrate the potential use of the TiO$_2$ nanoshells in electrochemical systems, we select cTiO$_2$ hollow spheres as a representative sample to investigate their lithium storage properties as anode materials for LIBs. The cyclic voltammograms (fig. S25) exhibit the characteristic Li$^+$ ion insertion/deinsertion behaviors for anatase TiO$_2$, with two redox peaks recorded at approximately 1.6 and 2.2 V versus Li$^+$/Li. Figure 6A shows typical discharge-charge voltage profiles within a cutoff voltage window of 1.0 to 3.0 V. There are two notable voltage plateaus at approximately 1.7 and 2.1 V versus Li$^+$/Li, which respectively correspond to the Li$^+$ ion insertion/deinsertion processes (*23*). The initial discharge and charge capacities are 184.1 and 142.8 mAh g^{-1}, respectively, with a high initial coulombic efficiency of 77.5%. After the first few cycles, the capacity quickly stabilizes, indicating that the electrochemical Li$^+$ ion insertion/deinsertion reactions are highly stable and reversible in the electrode. Figure 6B shows the cycling performance of cTiO$_2$ hollow spheres at a current density of 10 C (1 C = 173 mA g^{-1}). The capacity decays from initially 184.1 to 140.8 mAh g^{-1} in the second cycle, then to 138.6 mAh g^{-1} in the fifth cycle, and remains at 127.7 mAh g^{-1} after 1000 cycles, corresponding to a very low capacity fading rate of <0.01% per cycle from the second cycle onward. The long-term cycling stability of these TiO$_2$ hollow spheres is superior to that of other reported TiO$_2$-based anode materials (*11*, *12*, *46*–*48*). Moreover, the cTiO$_2$ hollow spheres can also be cycled with high stability at lower current rates of 1 and 5 C (fig. S26). As shown in Fig. 6C, the cTiO$_2$ hollow spheres also exhibit good rate capability at discharge-charge current rates ranging from 1 to 30 C. The average specific capacities are 196.2, 164.5, 127.4, 76.1, and 49.1 mAh g^{-1} at current rates of 1, 5, 10, 20, and 30 C, respectively. After the high-rate discharge-charge cycling, a specific capacity of 199.5 mAh g^{-1} can be restored when the current density is reduced back to 1 C. These results demonstrate that these mesoporous TiO$_2$ nanoshells have excellent electrochemical kinetics and lithium storage properties as potential anode materials. Moreover, a postmortem study of the material after the cycling test reveals that the hollow structure is retained after discharging/charging at 10 C for 100 cycles (fig. S27),

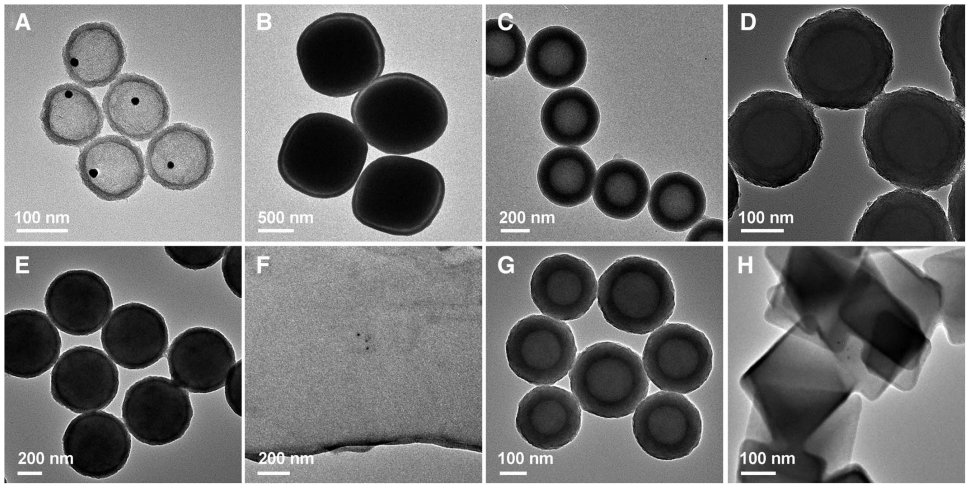

Fig. 5. TEM characterizations of TiO$_2$ yolk-shell and double-shell hollow structures and nanocomposites. (**A**) Au@TiO$_2$ yolk-shell nanospheres. (**B**) Fe$_2$O$_3$@TiO$_2$ yolk-shell cubes. (**C**) TiO$_2$-polymer double-shell nanospheres. (**D**) MSN@TiO$_2$ core-shell nanospheres. (**E**) PN@TiO$_2$ core-shell nanospheres. (**F**) GO@TiO$_2$ composite nanosheets. (**G**) CN@TiO$_2$ core-shell nanospheres. (**H**) MOF@TiO$_2$ core-shell particles.

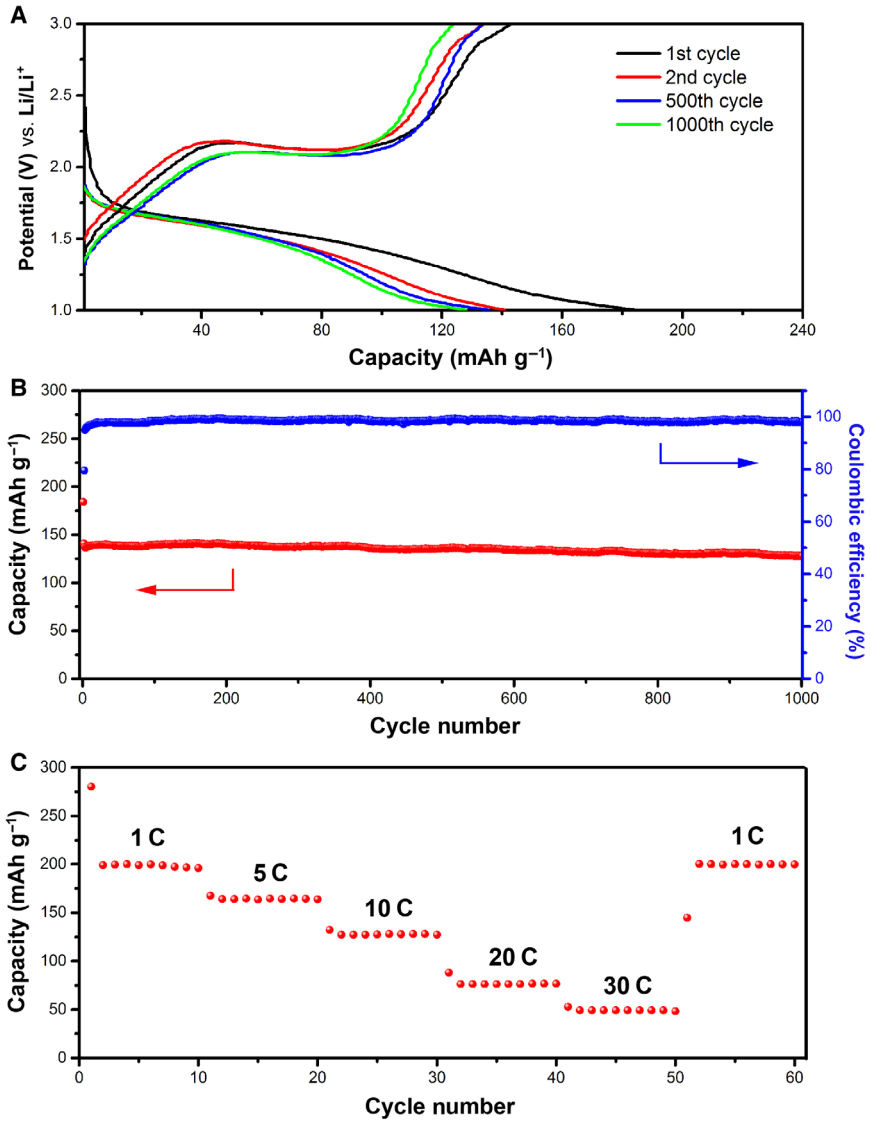

Fig. 6. Electrochemical characterizations of *c*TiO_2 hollow spheres as an anode material in LIBs. (**A**) Discharge-charge voltage profiles in the voltage range from 1.0 to 3.0 V at a current rate of 10 C. (**B**) Cycling performance and corresponding coulombic efficiency at a current rate of 10 C. (**C**) Rate performance at various current rates from 1 to 30 C. 1 C = 173 mA g^{-1}.

indicating the excellent structural robustness of these *c*TiO_2 hollow spheres.

DISCUSSION

In summary, a universal cooperative assembly-directed method is developed to form mesoporous TiO_2 shells on different particles at room temperature. A key feature of this new method is that HDA molecules serve as the soft template for mesostructured TiO_2, which allows successful growth of a layer of mesoporous TiO_2 (both amorphous and crystalline) on many functional nanomaterials irrespective of composition, shape, and size. This provides the platform for making many designed TiO_2-based hollow nanostructures, including hollow and yolk-shell structures with tailored cavity size and shell thickness and hybrid structures for different applications. It is foreseen that the present recipe will open up vast opportunities to precisely control the structure of TiO_2 nanocomposites for a wide range of applications. As a demonstration of their potential applications, *c*TiO_2 hollow spheres consisting of very small nanocrystals are shown to manifest improved lithium storage properties with remarkably stable capacity retention over 1000 cycles.

MATERIALS AND METHODS

Synthesis of SiO_2 nanospheres

Briefly, SiO_2 nanospheres were synthesized by a modified Stöber method. In a typical reaction, 23.5 ml of water, 63.3 ml of 2-propanol, and 13 ml of ammonia (25 to 28%) were mixed and heated in an oil

bath to 35°C. Then, 0.6 ml of TEOS (99%) was added dropwise to this solution, and the reaction was continued for 30 min under vigorous stirring to form the silica seeds. Then, 5 ml of TEOS was added dropwise to the reaction system. The reaction mixture was kept for 2 hours at 35°C. The SiO_2 nanospheres were isolated by centrifugation, washed with ethanol and water repeatedly, and finally dried in air.

Synthesis of SiO_2@TiO_2 core-shell spheres with *a*TiO_2 and *c*TiO_2 shells

For mesostructured TiO_2 coating, 0.08 g of as-prepared SiO_2 spheres was homogeneously dispersed in 9.74 ml of ethanol by ultrasonication, followed by the addition of 0.08 g of HDA (90%) and 0.2 ml of ammonia, and stirred at room temperature for 1 min to form uniform dispersion. Then, 0.2 ml of TIP (97%) was added to the dispersion under stirring, and the solution turned to white within 10 s. After reaction for 10 min, the product SiO_2@TiO_2/HDA core-shell particles were collected by centrifugation and then washed several times with water and ethanol. To prepare SiO_2@*a*TiO_2 yolk-shell spheres with mesoporous *a*TiO_2 shells, a solvothermal treatment of the SiO_2@TiO_2/HDA spheres was performed. The SiO_2@TiO_2/HDA spheres (0.02 g) were dispersed in a mixture of 20 ml of ethanol and 10 ml of water with an ammonia concentration of 0.5 M. Then, the resulting mixture was sealed in a Teflon-lined autoclave (50 ml in capacity) and heated at 160°C for 16 hours. Prolongation of the reaction time to 24 hours will generate completely hollow TiO_2 spheres with mesoporous *a*TiO_2 shells. To prepare SiO_2@*c*TiO_2 core-shell spheres with mesoporous *c*TiO_2 shells, a similar solvothermal treatment of the SiO_2@TiO_2/HDA spheres was performed but in the absence of ammonia. After that, the as-obtained SiO_2@*c*TiO_2 sample was calcined at 450°C for 2 hours in air and treated with a 10% HF solution to remove the silica template spheres and generate *c*TiO_2 hollow spheres.

Preparation of Au@TiO_2 yolk-shell nanospheres

Au@SiO_2 core-shell nanoparticles were prepared according to the method reported by Arnal *et al.* (*49*). For TiO_2 coating, 0.08 g of as-obtained Au@SiO_2 spheres was homogeneously dispersed in ethanol (9.74 ml) by ultrasonication, followed by the addition of 0.08 g of HDA and 0.2 ml of ammonia, and stirred at room temperature for 1 min to form uniform dispersion. Further stirring for 10 min was necessary, and Au@SiO_2@TiO_2 nanospheres were collected by centrifugation and then washed with water and ethanol several times. To prepare Au@TiO_2 yolk-shell nanospheres, a solvothermal treatment of the precursor beads was performed. The Au@SiO_2@TiO_2 spheres (0.02 g) were dispersed in a mixture of 20 ml of ethanol and 10 ml of water with an ammonia concentration of 0.5 M. Then, the resulting mixture was sealed in a Teflon-lined autoclave (50 ml in capacity) and heated at 160°C for 16 hours. After centrifugation and ethanol washing, 0.01 g of the obtained pink powder was dispersed in 30 ml of 0.05 M aqueous NaOH solution. Then, the resulting mixture was sealed in a Teflon-lined autoclave (50 ml) and heated at 85°C for 1.5 hours. The Au@TiO_2 nanospheres were isolated by centrifugation, washed repeatedly with ethanol and water, and finally dried in air for characterization.

Synthesis of Fe_2O_3@TiO_2 yolk-shell cubes

Uniform Fe_2O_3 cubes were synthesized by the method developed by Sugimoto *et al.* (*50*). Silica coating on Fe_2O_3 cubes was achieved by a modified Stöber method. Briefly, 0.15 g of Fe_2O_3 cubes was dispersed into 65 ml of ethanol and 6.5 ml of H_2O through ultrasonication, followed by the addition of 6 ml of ammonia solution. TEOS (0.5 ml) dissolved in 4.5 ml of absolute ethanol was slowly added into the mixture at a rate of 1 ml min^{-1} under magnetic stirring. The reaction was continued for 6 hours before the product was collected by centrifugation, followed by washing and drying at 70°C overnight. For TiO_2 coating, 0.1 g of as-obtained Fe_2O_3@SiO_2 cubes was homogeneously dispersed in ethanol (9.74 ml) by ultrasonication, followed by the addition of 0.08 g of HDA and 0.2 ml of ammonia, and then stirred at room temperature for 1 min to form uniform dispersion. Then, 0.1 ml of TIP was added to the dispersion under stirring. Stirring for another 10 min was necessary, and then Fe_2O_3@SiO_2@TiO_2 cubes were collected by centrifugation. To prepare Fe_2O_3@TiO_2 yolk-shell spheres, a solvothermal treatment of Fe_2O_3@SiO_2@TiO_2 cubes was performed. The Fe_2O_3@SiO_2@TiO_2 precursor cubes (0.02 g) were dispersed in a mixture of 20 ml of ethanol and 10 ml of water with an ammonia concentration of 0.5 M. Then, the resulting mixture was sealed in a Teflon-lined autoclave (50 ml) and heated at 160°C for 16 hours.

Synthesis of TiO_2-polymer double-shell hollow spheres

Briefly, 0.1 g of as-obtained hollow TiO_2 spheres was homogeneously dispersed in deionized water (7.04 ml) by ultrasonication, followed by the addition of 0.23 g of CTAB, 0.035 g of resorcinol, 2.82 ml of ethanol, and 0.01 ml of ammonia, and stirred at 35°C for 1 min to form uniform dispersion. Then, 0.05 ml of a formalin solution was added to the dispersion under stirring. The mixture was cooled to room temperature after 6 hours and then aged at room temperature overnight without stirring. The TiO_2@polymer product was collected by centrifugation and washed with water and ethanol several times.

Synthesis of MSNs and MSN@TiO_2 nanospheres

MSNs were synthesized by the method developed by Lu *et al.* (*51*). For TiO_2 coating, 0.06 g of as-obtained MSNs was homogeneously dispersed in ethanol (9.74 ml) by ultrasonication, followed by the addition of 0.08 g of HDA and 0.2 ml of ammonia. The mixture was then stirred at room temperature for 1 min to form uniform dispersion. Then, 0.2 ml of TIP was added to the dispersion under stirring. After stirring for another 10 min, MSN@TiO_2 nanospheres were collected by centrifugation and then washed with water and ethanol several times.

Synthesis of PNs and PN@TiO_2 nanospheres

PNs were synthesized by the method developed by Liu *et al.* (*52*). For TiO_2 coating, 0.04 g of as-obtained PNs was homogeneously dispersed in ethanol (9.74 ml) by ultrasonication, followed by the addition of 0.08 g of HDA and 0.2 ml of ammonia, and stirred for 1 min to form uniform dispersion. Then, 0.2 ml of TIP was added to the dispersion under stirring. After stirring for 10 min, PN@TiO_2 nanospheres were collected by centrifugation and then washed with water and ethanol several times.

Synthesis of GO and GO@TiO_2 nanosheets

GO nanosheets were prepared according to Hummers method (*53*). For TiO_2 coating, 0.005 g of as-obtained GO was homogeneously dispersed in ethanol (9.74 ml) by ultrasonication, followed by the addition of 0.08 g of HDA and 0.2 ml of ammonia, and then stirred at room temperature for 1 min to form uniform dispersion. Then, 0.04 ml of TIP was added to the dispersion under stirring. After stirring for

10 min, GO@TiO_2 nanosheets were collected by centrifugation and then washed with water and ethanol several times.

Synthesis of CNs and CN@TiO_2 nanospheres

CNs were synthesized according to Sun and Li's method (*54*). For TiO_2 coating, 0.02 g of as-obtained CNs was homogeneously dispersed in ethanol (9.74 ml) by ultrasonication, followed by the addition of 0.08 g of HDA and 0.2 ml of ammonia, and then stirred at room temperature for 1 min to form uniform dispersion. Then, 0.04 ml of TIP was added to the dispersion under stirring. After stirring for 10 min, CN@TiO_2 nanospheres were collected by centrifugation and then washed with water and ethanol several times.

Synthesis of MOF and MOF@TiO_2 nanocrystals

MOF nanocrystals were synthesized according to the method by Lu *et al.* (*55*). For TiO_2 coating, 0.08 g of as-obtained MOF crystals was homogeneously dispersed in ethanol (9.74 ml) by ultrasonication, followed by the addition of 0.08 g of HDA and 0.2 ml of ammonia, and then stirred at room temperature for 1 min to form uniform dispersion. Then, 0.2 ml of TIP was added to the dispersion under stirring. After stirring for 10 min, MOF@TiO_2 nanocrystals were collected by centrifugation and then washed with water and ethanol several times.

Materials characterization

The crystal phase of the products was examined by XRD on a Bruker D2 Phaser x-ray diffractometer. A field-emission scanning electron microscope (FESEM; JEOL-6700F) and a transmission electron microscope (TEM; JEOL, JEM-2010) were used for morphology characterizations. The nitrogen sorption measurement was carried on Autosorb-6B at liquid-nitrogen temperature. The particle size was measured by photon correlation spectroscopy using a Nano ZS90 laser particle analyzer (Malvern Instruments) at 25°C. FTIR spectra were recorded with an FTIR-Digilab FTS 3100 spectrometer.

Electrochemical measurements

Electrochemical measurements were carried out using CR2032 coin-type half-cells. The working electrode consisted of active material (that is, *c*TiO_2 hollow spheres), carbon black (Super P Li), and polymer binder (polyvinylidene fluoride) in a weight ratio of 70:20:10. Lithium foil was used as both the counter electrode and the reference electrode. $LiPF_6$ (1 M) in a 50:50 (w/w) mixture of ethylene carbonate and diethyl carbonate was used as the electrolyte. Cell assembly was carried out in an Ar-filled glove box with moisture and oxygen concentrations below 1.0 ppm. The galvanostatic charge-discharge tests were performed on a Neware battery test system.

SUPPLEMENTARY MATERIALS

Supplementary material for this article is available at http://advances.sciencemag.org/cgi/content/full/2/3/e1501554/DC1

Fig. S1. FESEM characterizations of SiO_2@TiO_2/HDA core-shell spheres and SiO_2@*a*TiO_2 yolk-shell spheres.
Fig. S2. DLS analysis of SiO_2 templates and SiO_2@TiO_2/HDA spheres.
Fig. S3. Small-angle XRD analysis of the particles with mesostructured TiO_2 shells.
Fig. S4. FTIR study on the interactions between TiO_2 and HDA.
Fig. S5. Wide-angle XRD analysis of the particles with *a*TiO_2 shells.
Fig. S6. N_2 sorption analysis of SiO_2@*a*TiO_2 and SiO_2@TiO_2/HDA samples.
Fig. S7. FTIR study of surfactant removal.
Fig. S8. TEM characterizations of SiO_2@TiO_2/HDA spheres and *a*TiO_2 hollow spheres.
Fig. S9. N_2 sorption analysis of *a*TiO_2 hollow spheres.
Fig. S10. FESEM characterizations of mesoporous *a*TiO_2 hollow spheres.
Fig. S11. TEM characterizations of SiO_2@*c*TiO_2 spheres.
Fig. S12. FTIR and N_2 sorption analysis of SiO_2@*c*TiO_2 spheres.
Fig. S13. Wide-angle XRD analysis of the particles with *c*TiO_2 shells.
Fig. S14. N_2 sorption analysis of *c*TiO_2 hollow spheres.
Fig. S15. Elemental analysis of *c*TiO_2 hollow spheres.
Fig. S16. TEM and XRD characterizations of SiO_2@TiO_2/HDA spheres treated with 0.1 M HCl and 0.1 M NaOH solutions.
Fig. S17. TEM characterizations of the formation process of Au@TiO_2 yolk-shell spheres.
Fig. S18. FESEM and TEM characterizations of the formation process of Fe_2O_3@TiO_2 yolk-shell particles.
Fig. S19. FESEM and TEM characterizations of the formation process of TiO_2-polymer double-shell hollow spheres.
Fig. S20. FESEM characterizations of different TiO_2 core-shell composites.
Fig. S21. FESEM characterizations of CN and MOF templates.
Fig. S22. Wide-angle XRD analysis of different functional cores.
Fig. S23. TEM characterizations of CNT@TiO_2 nanofibers.
Fig. S24. TEM characterizations and small-angle XRD analysis of different TiO_2 core-shell composites.
Fig. S25. Cyclic voltammetry characterization of *c*TiO_2 hollow spheres.
Fig. S26. Electrochemical characterizations of *c*TiO_2 hollow spheres as an anode material in LIBs.
Fig. S27. FESEM characterization of *c*TiO_2 hollow spheres before and after cycling test.

REFERENCES AND NOTES

1. X. Chen, S. S. Mao, Titanium dioxide nanomaterials: Synthesis, properties, modifications, and applications. *Chem. Rev.* **107**, 2891–2959 (2007).
2. H. G. Moon, Y.-S. Shim, H. W. Jang, J.-S. Kim, K. J. Choi, C.-Y. Kang, J.-W. Choi, H.-H. Park, S.-J. Yoon, Highly sensitive CO sensors based on cross-linked TiO_2 hollow hemispheres. *Sens. Actuators B* **149**, 116–121 (2010).
3. N. Yang, Y. Liu, H. Wen, Z. Tang, H. Zhao, Y. Li, D. Wang, Photocatalytic properties of graphdiyne and graphene modified TiO_2: From theory to experiment. *ACS Nano* **7**, 1504–1512 (2013).
4. H. Liu, J. Bong Joo, M. Dahl, L. Fu, Z. Zeng, Y. Yin, Crystallinity control of TiO_2 hollow shells through resin-protected calcination for enhanced photocatalytic activity. *Energ. Environ. Sci.* **8**, 286–296 (2015).
5. L. Cao, D. Chen, R. A. Caruso, Surface-metastable phase-initiated seeding and Ostwald ripening: A facile fluorine-free process towards spherical fluffy core/shell, yolk/shell, and hollow anatase nanostructures. *Angew. Chem. Int. Ed.* **52**, 10986–10991 (2013).
6. S. Liu, J. Yu, M. Jaroniec, Tunable photocatalytic selectivity of hollow TiO_2 microspheres composed of anatase polyhedra with exposed {001} facets. *J. Am. Chem. Soc.* **132**, 11914–11916 (2010).
7. X. Feng, K. Zhu, A. J. Frank, C. A. Grimes, T. E. Mallouk, Rapid charge transport in dye-sensitized solar cells made from vertically aligned single-crystal rutile TiO_2 nanowires. *Angew. Chem. Int. Ed.* **51**, 2727–2730 (2012).
8. J. Du, X. Lai, N. Yang, J. Zhai, D. Kisailus, F. Su, D. Wang, L. Jiang, Hierarchically ordered macro-mesoporous TiO_2-graphene composite films: Improved mass transfer, reduced charge recombination, and their enhanced photocatalytic activities. *ACS Nano* **5**, 590–596 (2011).
9. U. Bach, D. Lupo, P. Comte, J. E. Moser, F. Weissörtel, J. Salbeck, H. Spreitzer, M. Grätzel, Solid-state dye-sensitized mesoporous TiO_2 solar cells with high photon-to-electron conversion efficiencies. *Nature* **395**, 583–585 (1998).
10. X.-Y. Yu, H. B. Wu, L. Yu, F.-X. Ma, X. W. Lou, Rutile TiO_2 submicroboxes with superior lithium storage properties. *Angew. Chem. Int. Ed.* **54**, 4001–4004 (2015).
11. G. Zhang, H. B. Wu, T. Song, U. Paik, X. W. Lou, TiO_2 hollow spheres composed of highly crystalline nanocrystals exhibit superior lithium storage properties. *Angew. Chem. Int. Ed.* **53**, 12590–12593 (2014).
12. H. Ren, R. Yu, J. Wang, Q. Jin, M. Yang, D. Mao, D. Kisailus, H. Zhao, D. Wang, Multishelled TiO_2 hollow microspheres as anodes with superior reversible capacity for lithium ion batteries. *Nano Lett.* **14**, 6679–6684 (2014).
13. H. Hu, L. Yu, X. Gao, Z. Lin, X. W. Lou, Hierarchical tubular structures constructed from ultrathin TiO_2(B) nanosheets for highly reversible lithium storage. *Energ. Environ. Sci.* **8**, 1480–1483 (2015).
14. I. Lee, J. B. Joo, Y. Yin, F. Zaera, A yolk@shell nanoarchitecture for Au/TiO_2 catalysts. *Angew. Chem. Int. Ed.* **50**, 10208–10211 (2011).
15. J. B. Joo, I. Lee, M. Dahl, G. D. Moon, F. Zaera, Y. Yin, Controllable synthesis of mesoporous TiO_2 hollow shells: Toward an efficient photocatalyst. *Adv. Funct. Mater.* **23**, 4246–4254 (2013).
16. A. F. Demirörs, A. van Blaaderen, A. Imhof, A general method to coat colloidal particles with titania. *Langmuir* **26**, 9297–9303 (2010).

17. X. W. Lou, L. A. Archer, A general route to nonspherical anatase TiO_2 hollow colloids and magnetic multifunctional particles. *Adv. Mater.* **20**, 1853–1858 (2008).
18. F. Caruso, X. Shi, R. A. Caruso, A. Susha, Hollow titania spheres from layered precursor deposition on sacrificial colloidal core particles. *Adv. Mater.* **13**, 740–744 (2001).
19. H. Sakai, T. Kanda, H. Shibata, T. Ohkubo, M. Abe, Preparation of highly dispersed core/shell-type titania nanocapsules containing a single Ag nanoparticle. *J. Am. Chem. Soc.* **128**, 4944–4945 (2006).
20. Y. Lu, Y. Yin, Y. Xia, Preparation and characterization of micrometer-sized "egg shells". *Adv. Mater.* **13**, 271–274 (2001).
21. D. Chen, L. Cao, F. Huang, P. Imperia, Y.-B. Cheng, R. A. Caruso, Synthesis of monodisperse mesoporous titania beads with controllable diameter, high surface areas, and variable pore diameters (14–23 nm). *J. Am. Chem. Soc.* **132**, 4438–4444 (2010).
22. J. B. Joo, M. Dahl, N. Li, F. Zaera, Y. Yin, Tailored synthesis of mesoporous TiO_2 hollow nanostructures for catalytic applications. *Energ. Environ. Sci.* **6**, 2082–2092 (2013).
23. Z. Wang, X. W. Lou, TiO_2 nanocages: Fast synthesis, interior functionalization and improved lithium storage properties. *Adv. Mater.* **24**, 4124–4129 (2012).
24. W. Li, J. Yang, Z. Wu, J. Wang, B. Li, S. Feng, Y. Deng, F. Zhang, D. Zhao, A versatile kinetics-controlled coating method to construct uniform porous TiO_2 shells for multifunctional core–shell structures. *J. Am. Chem. Soc.* **134**, 11864–11867 (2012).
25. J. B. Joo, Q. Zhang, I. Lee, M. Dahl, F. Zaera, Y. Yin, Mesoporous anatase titania hollow nanostructures though silica-protected calcination. *Adv. Funct. Mater.* **22**, 166–174 (2012).
26. C. Detavernier, J. Dendooven, S. Pulinthanathu Sree, K. F. Ludwig, J. A. Martens, Tailoring nanoporous materials by atomic layer deposition. *Chem. Soc. Rev.* **40**, 5242–5253 (2011).
27. R. Liu, A. Sen, Controlled synthesis of heterogeneous metal–titania nanostructures and their applications. *J. Am. Chem. Soc.* **134**, 17505–17512 (2012).
28. C. J. Brinker, G. W. Scherer, *Sol-Gel Science: The Physics and Chemistry of Sol-Gel Processing* (Academic Press, New York, 1990).
29. A. C. Pierre, G. M. Pajonk, Chemistry of aerogels and their applications. *Chem. Rev.* **102**, 4243–4265 (2002).
30. Y. Yin, Y. Lu, Y. Sun, Y. Xia, Silver nanowires can be directly coated with amorphous silica to generate well-controlled coaxial nanocables of silver/silica. *Nano Lett.* **2**, 427–430 (2002).
31. W. Dong, Y. Sun, C. W. Lee, W. Hua, X. Lu, Y. Shi, S. Zhang, J. Chen, D. Zhao, Controllable and repeatable synthesis of thermally stable anatase nanocrystal–silica composites with highly ordered hexagonal mesostructures. *J. Am. Chem. Soc.* **129**, 13894–13904 (2007).
32. D. Zhao, J. Feng, Q. Huo, N. Melosh, G. H. Fredrickson, B. F. Chmelka, G. D. Stucky, Triblock copolymer syntheses of mesoporous silica with periodic 50 to 300 angstrom pores. *Science* **279**, 548–552 (1998).
33. D. Zhao, Q. Huo, J. Feng, B. F. Chmelka, G. D. Stucky, Nonionic triblock and star diblock copolymer and oligomeric surfactant syntheses of highly ordered, hydrothermally stable, mesoporous silica structures. *J. Am. Chem. Soc.* **120**, 6024–6036 (1998).
34. S. H. Joo, J. Y. Park, C.-K. Tsung, Y. Yamada, P. Yang, G. A. Somorjai, Thermally stable Pt/mesoporous silica core–shell nanocatalysts for high-temperature reactions. *Nat. Mater.* **8**, 126–131 (2009).
35. I. Gorelikov, N. Matsuura, Single-step coating of mesoporous silica on cetyltrimethyl ammonium bromide-capped nanoparticles. *Nano Lett.* **8**, 369–373 (2008).
36. J. Kim, H. S. Kim, N. Lee, T. Kim, H. Kim, T. Yu, C. Song, W. K. Moon, T. Hyeon, Multifunctional uniform nanoparticles composed of a magnetite nanocrystal core and a mesoporous silica shell for magnetic resonance and fluorescence imaging and for drug delivery. *Angew. Chem. Int. Ed.* **47**, 8438–8441 (2008).
37. J. Dou, H. C. Zeng, Targeted synthesis of silicomolybdic acid (keggin acid) inside mesoporous silica hollow spheres for Friedel–Crafts alkylation. *J. Am. Chem. Soc.* **134**, 16235–16246 (2012).
38. Y. Deng, D. Qi, C. Deng, X. Zhang, D. Zhao, Superparamagnetic high-magnetization microspheres with an Fe_3O_4@SiO_2 core and perpendicularly aligned mesoporous SiO_2 shell for removal of microcystins. *J. Am. Chem. Soc.* **130**, 28–29 (2008).
39. X. Li, L. Zhou, Y. Wei, A. M. El-Toni, F. Zhang, D. Zhao, Anisotropic growth-induced synthesis of dual-compartment Janus mesoporous silica nanoparticles for bimodal triggered drugs delivery. *J. Am. Chem. Soc.* **136**, 15086–15092 (2014).
40. V. Cauda, A. Schlossbauer, J. Kecht, A. Zürner, T. Bein, Multiple core–shell functionalized colloidal mesoporous silica nanoparticles. *J. Am. Chem. Soc.* **131**, 11361–11370 (2009).
41. B. Guan, X. Wang, Y. Xiao, Y. Liu, Q. Huo, A versatile cooperative template-directed coating method to construct uniform microporous carbon shells for multifunctional core–shell nanocomposites. *Nanoscale* **5**, 2469–2475 (2013).
42. G.-N. Zhu, Y.-G. Wang, Y.-Y. Xia, Ti-based compounds as anode materials for Li-ion batteries. *Energ. Environ. Sci.* **5**, 6652–6667 (2012).
43. Z. Wang, L. Zhou, X. W. Lou, Metal oxide hollow nanostructures for lithium-ion batteries. *Adv. Mater.* **24**, 1903–1911 (2012).
44. X. Lai, J. E. Halpert, D. Wang, Recent advances in micro-/nano-structured hollow spheres for energy applications: From simple to complex systems. *Energ. Environ. Sci.* **5**, 5604–5618 (2012).
45. J. B. Joo, Q. Zhang, M. Dahl, I. Lee, J. Goebl, F. Zaera, Y. Yin, Control of the nanoscale crystallinity in mesoporous TiO_2 shells for enhanced photocatalytic activity. *Energ. Environ. Sci.* **5**, 6321–6327 (2012).
46. T. Xia, W. Zhang, J. B. Murowchick, G. Liu, X. Chen, A facile method to improve the photocatalytic and lithium-ion rechargeable battery performance of TiO_2 nanocrystals. *Adv. Energ. Mater.* **3**, 1516–1523 (2013).
47. J. Luo, X. Xia, Y. Luo, C. Guan, J. Liu, X. Qi, C. F. Ng, T. Yu, H. Zhang, H. J. Fan, Rationally designed hierarchical TiO_2@Fe_2O_3 hollow nanostructures for improved lithium ion storage. *Adv. Energ. Mater.* **3**, 737–743 (2013).
48. W. Li, F. Wang, S. Feng, J. Wang, Z. Sun, B. Li, Y. Li, J. Yang, A. A. Elzatahry, Y. Xia, D. Zhao, Sol–gel design strategy for ultradispersed TiO_2 nanoparticles on graphene for high-performance lithium ion batteries. *J. Am. Chem. Soc.* **135**, 18300–18303 (2013).
49. P. M. Arnal, M. Comotti, F. Schüth, High-temperature-stable catalysts by hollow sphere encapsulation. *Angew. Chem. Int. Ed.* **45**, 8224–8227 (2006).
50. T. Sugimoto, M. M. Khan, A. Muramatsu, H. Itoh, Formation mechanism of monodisperse peanut-type α-Fe_2O_3 particles from condensed ferric hydroxide gel. *Colloids Surf. A* **79**, 233–247 (1993).
51. F. Lu, S.-H. Wu, Y. Hung, C.-Y. Mou, Size effect on cell uptake in well-suspended, uniform mesoporous silica nanoparticles. *Small* **5**, 1408–1413 (2009).
52. J. Liu, S. Z. Qiao, H. Liu, J. Chen, A. Orpe, D. Zhao, G. Q. (Max) Lu, Extension of the Stöber method to the preparation of monodisperse resorcinol–formaldehyde resin polymer and carbon spheres. *Angew. Chem. Int. Ed.* **50**, 5947–5951 (2011).
53. W. S. Hummers Jr., R. E. Offeman, Preparation of graphitic oxide. *J. Am. Chem. Soc.* **80**, 1339 (1958).
54. X. Sun, Y. Li, Colloidal carbon spheres and their core/shell structures with noble-metal nanoparticles. *Angew. Chem. Int. Ed.* **43**, 597–601 (2004).
55. G. Lu, C. Cui, W. Zhang, Y. Liu, F. Huo, Synthesis and self-assembly of monodispersed metal-organic framework microcrystals. *Chem. Asian J.* **8**, 69–72 (2013).

Acknowledgments: We thank Z. Li for useful discussion and the independent measurement of battery properties. **Funding:** X.W.L. acknowledges support from the Ministry of Education of Singapore through Academic Research Fund (AcRF) Tier-1 Funding (M4011154.120; RG12/13). J.L. acknowledges support by NSF Division of Materials Research (DMR)–1410636 and DMR-1120901. **Author contributions:** X.W.L. and B.Y.G. conceived the idea. B.Y.G. carried out the materials synthesis and electrochemical testing. L.Y. and B.Y.G. characterized the materials. B.Y.G., J.L., and X.W.L. cowrote the manuscript. **Competing interests:** The authors declare that they have no competing interests. **Data and materials availability:** All data needed to evaluate the conclusions in the paper are present in the paper and/or the Supplementary Materials. Additional data related to this paper may be requested from the authors.

Submitted 2 November 2015
Accepted 5 January 2016
Published 4 March 2016
10.1126/sciadv.1501554

Citation: B. Y. Guan, L. Yu, J. Li, X. W. Lou, A universal cooperative assembly-directed method for coating of mesoporous TiO2 nanoshells with enhanced lithium storage properties. *Sci. Adv.* **2**, e1501554 (2016).

A universal cooperative assembly-directed method for coating of mesoporous TiO_2 nanoshells with enhanced lithium storage properties
Bu Yuan Guan, Le Yu, Ju Li and Xiong Wen (David) Lou (March 4, 2016)
Sci Adv 2016, 2:.
doi: 10.1126/sciadv.1501554

Science Advances

AAAS

advances.sciencemag.org/cgi/content/full/2/3/e1501554/DC1

Supplementary Materials for

A universal cooperative assembly-directed method for coating of mesoporous TiO_2 nanoshells with enhanced lithium storage properties

Bu Yuan Guan, Le Yu, Ju Li, Xiong Wen (David) Lou

Published 4 March 2016, *Sci. Adv.* **2**, e1501554 (2016)
DOI: 10.1126/sciadv.1501554

The PDF file includes:

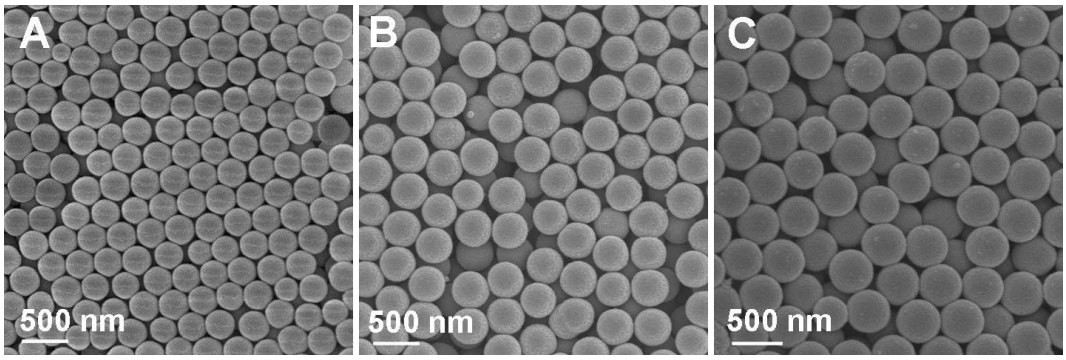

Fig. S1. FESEM characterizations of SiO_2@TiO_2/HDA core-shell spheres and SiO_2@*a*TiO_2 yolk-shell spheres. (**A**) SiO_2 template spheres, (**B**) SiO_2@TiO_2/HDA core-shell spheres, and (**C**) SiO_2@*a*TiO_2 yolk-shell spheres.

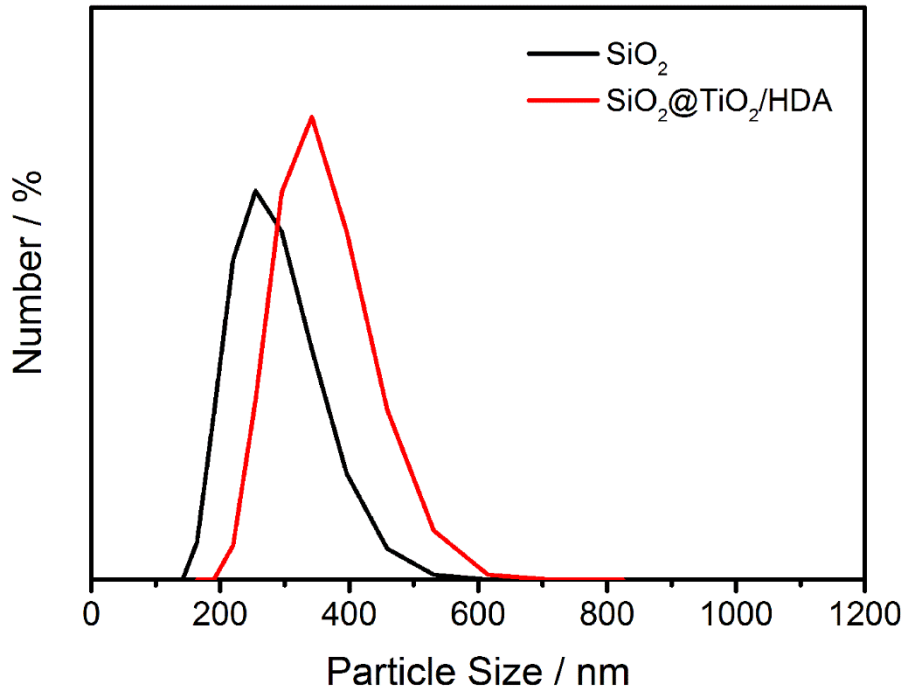

Fig. S2. DLS analysis of SiO_2 templates and SiO_2@TiO_2/HDA spheres. Hydrodynamic diameter of the SiO_2 and SiO_2@TiO_2/HDA spheres.

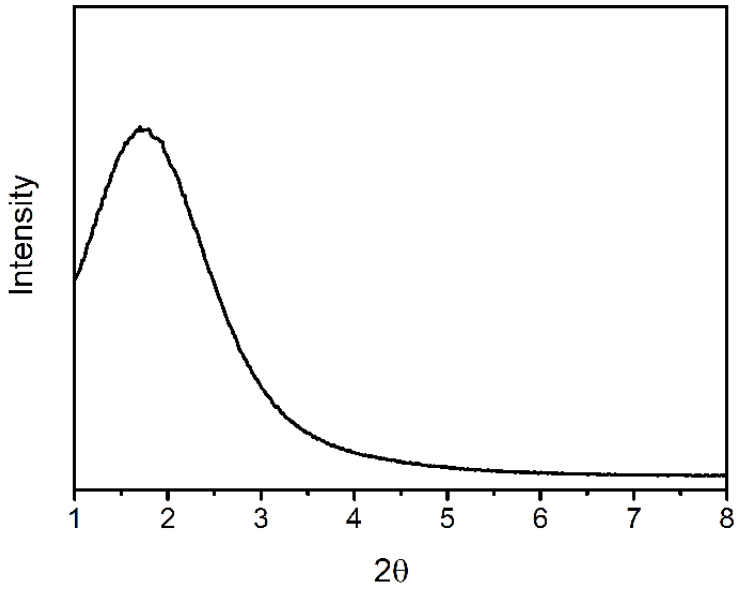

Fig. S3. Small-angle XRD analysis. XRD pattern of SiO_2@TiO_2/HDA spheres with mesostructured shells.

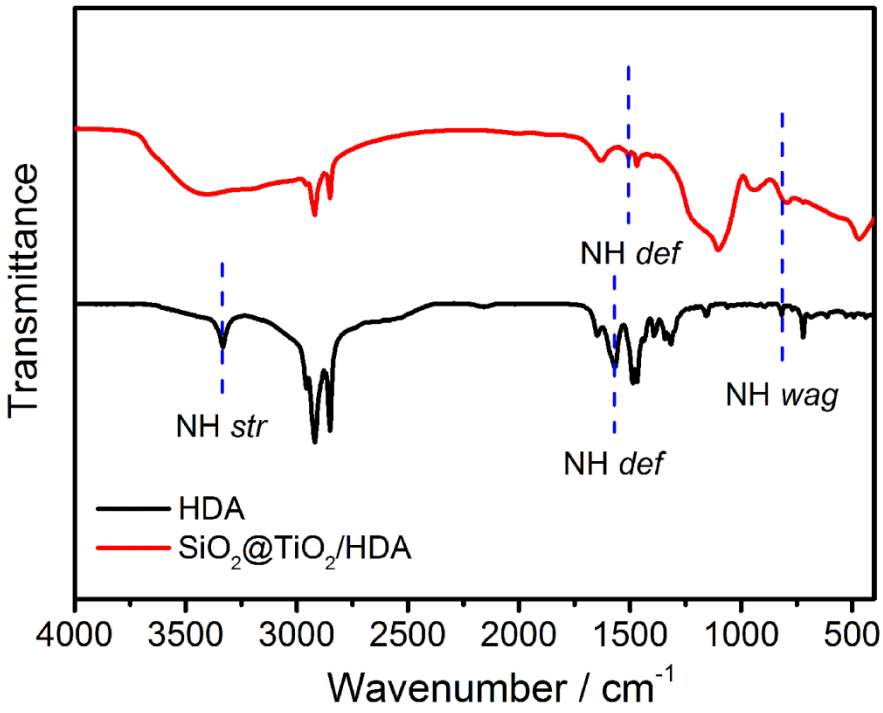

Fig. S4. FTIR study on the interactions between TiO_2 and HDA. FTIR spectra of SiO_2@TiO_2/HDA particles and HDA molecules.

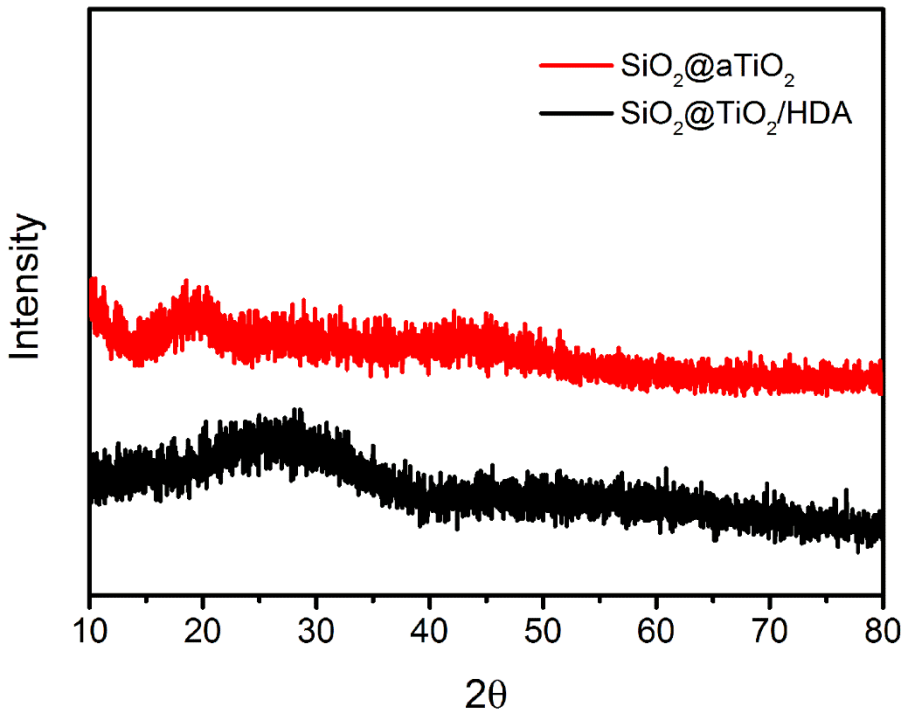

Fig. S5. Wide-angle XRD analysis of the particles with amorphous TiO_2 shells. XRD patterns of SiO_2@*a*TiO_2 and SiO_2@TiO_2/HDA nanospheres.

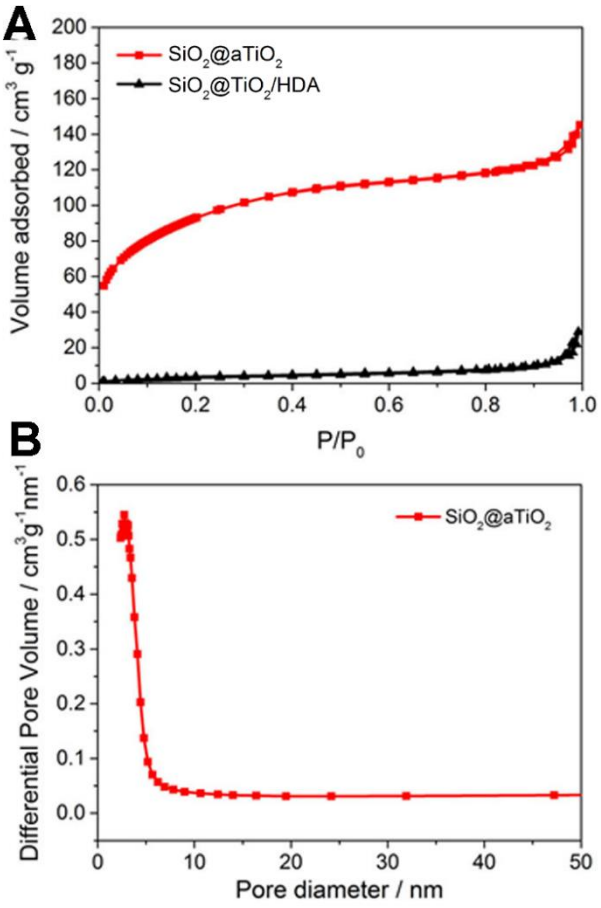

Fig. S6. N_2 sorption analysis of SiO_2@*a*TiO_2 and SiO_2@TiO_2/HDA samples. (**A**) N_2 adsorption-desorption isotherms of SiO_2@*a*TiO_2 and SiO_2@TiO_2/HDA nanospheres and (**B**) pore-size distribution of SiO_2@*a*TiO_2 nanospheres.

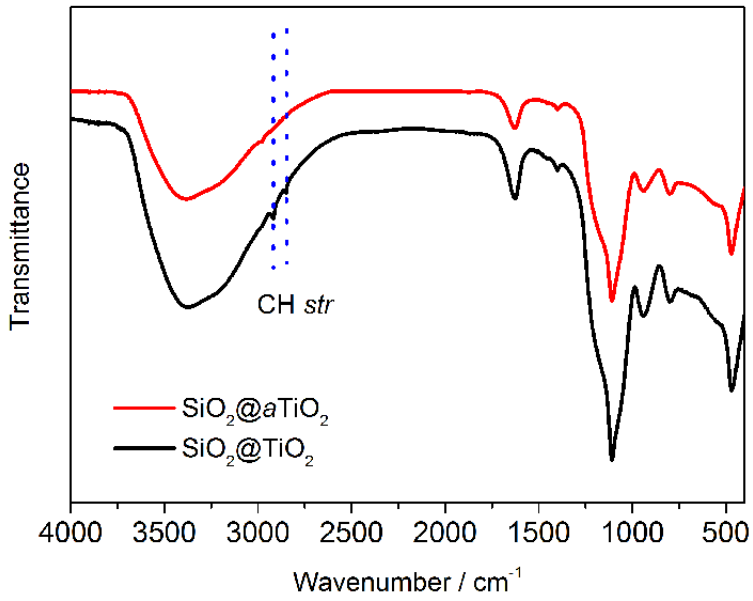

Fig. S7. FTIR study of surfactant removal. FTIR spectra of yolk-shell SiO_2@*a*TiO_2 spheres obtained after hydrothermal treatment and SiO_2@TiO_2/HDA particles after extraction process five times in ethanol.

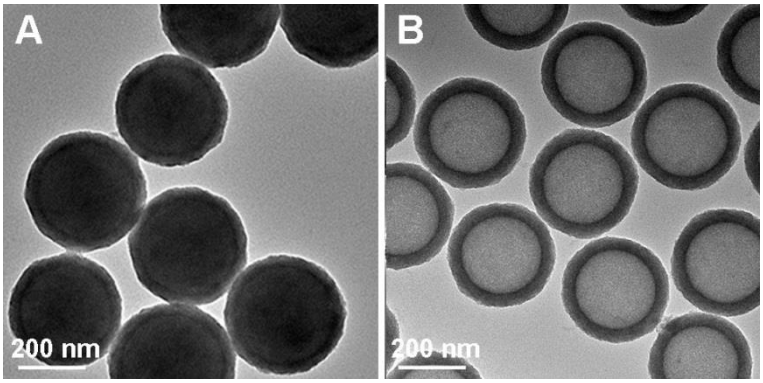

Fig. S8. TEM characterization. (**A**) SiO_2@TiO_2/HDA core-shell nanospheres, and (**B**) *a*TiO_2 hollow nanospheres with amorphous shells after solvothermal treatment in ammonia solution at 160 ˚C for 24 h.

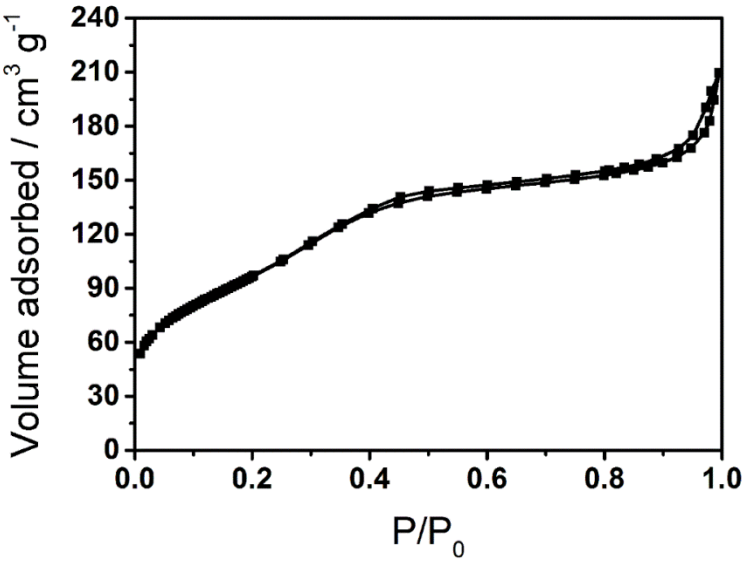

Fig. S9. N_2 sorption analysis of *a*TiO_2 hollow spheres.

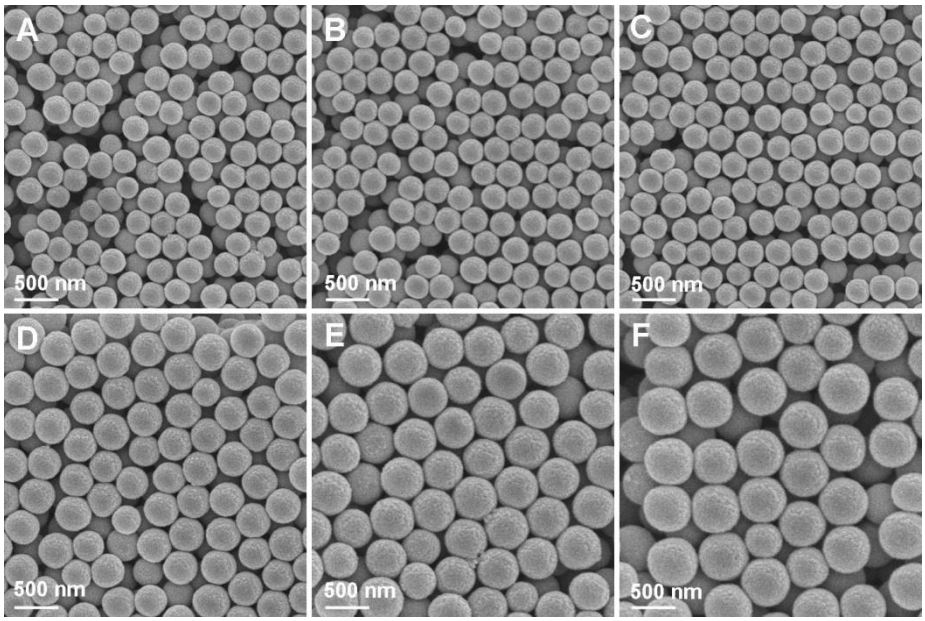

Fig. S10. FESEM characterizations of mesoporous *a*TiO_2 hollow spheres. (**A** to **C**) *a*TiO_2 hollow spheres with identical hollow core size of about 230 nm but varied shell thicknesses: (**A**) 8 nm, (**B**) 41 nm, and (**C**) 54 nm. (**D** to **F**) *a*TiO_2 hollow spheres with average outer (inner) diameter of (**D**) 300 (270) nm, (**E**) 410 (325) nm, and (**F**) 680 (475) nm.

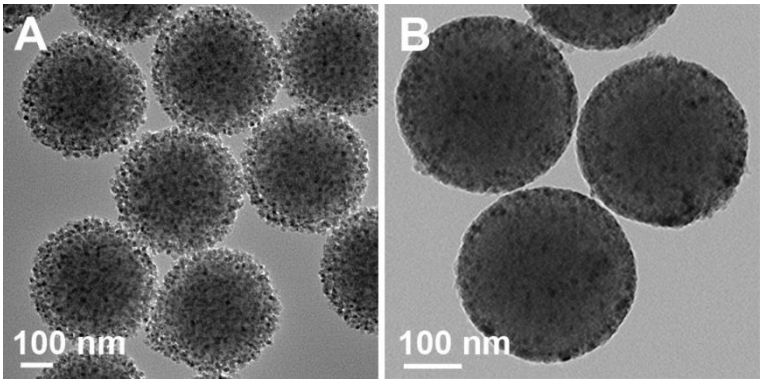

Fig. S11. TEM characterization. (**A**) SiO_2@*c*TiO_2 core-shell nanospheres with crystalline shells after solvothermal treatment without ammonia, and (**B**) SiO_2@*c*TiO_2 core-shell nanospheres after calcination process in air at 450 ^oC.

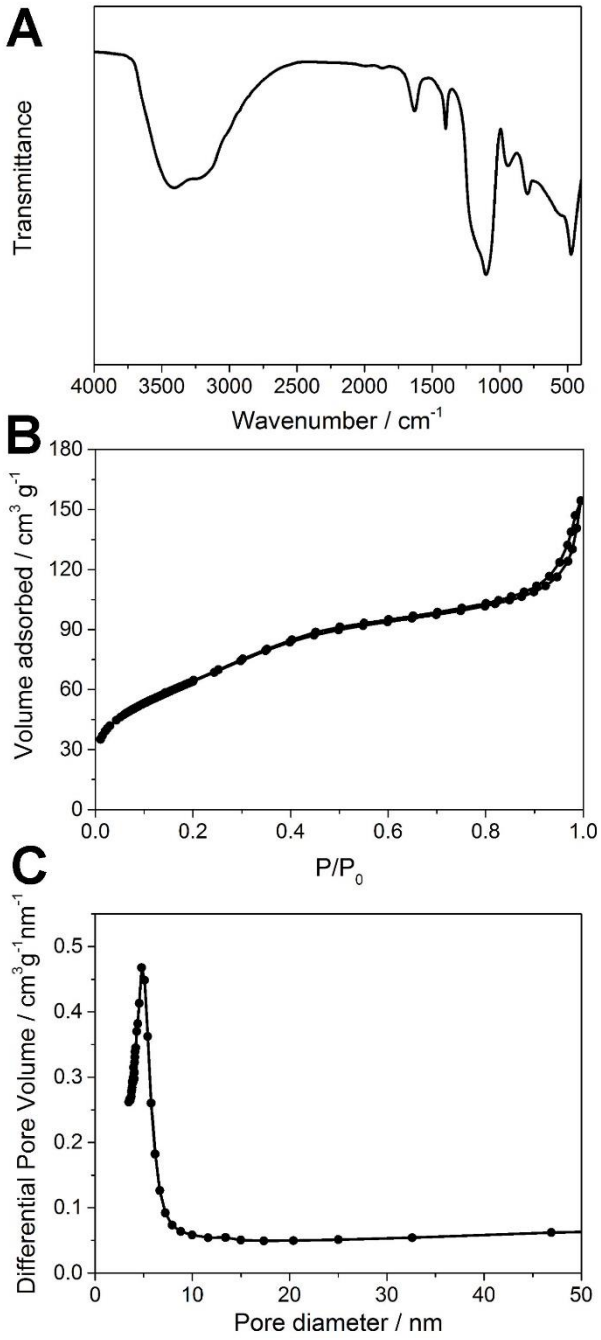

Fig. S12. FTIR and N_2 sorption analysis of SiO_2@*c*TiO_2 spheres. (**A**) FTIR spectrum of SiO_2@*c*TiO_2 spheres obtained after hydrothermal treatment without ammonia. (**B**) N_2 adsorption-desorption isotherm and (**C**) pore-size distribution of SiO_2@*c*TiO_2 spheres.

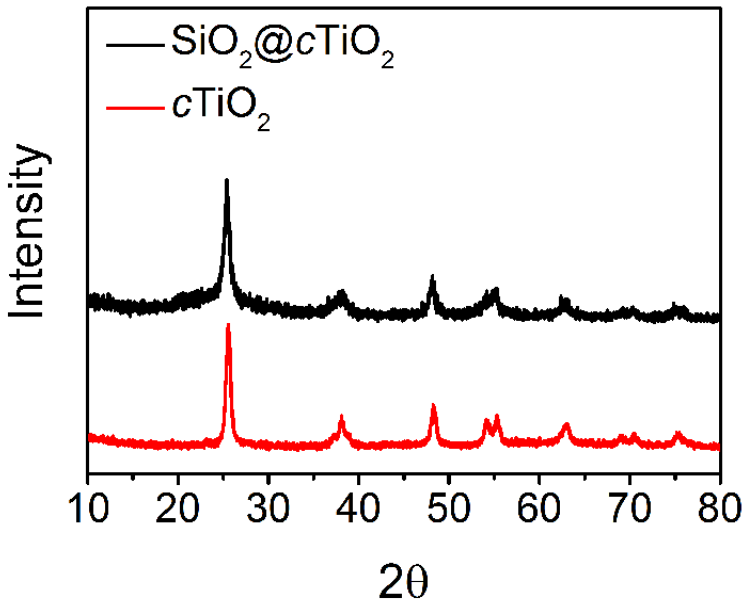

Fig. S13. Wide-angle XRD analysis of the particles with crystalline TiO_2 shells. XRD patterns of SiO_2@*c*TiO_2 core-shell nanospheres and *c*TiO_2 hollow nanospheres with crystalline shells. The different degrees of crystallinity between the TiO_2 samples obtained in alkaline and neutral conditions might be due to the suppressing effect of dissolving silica on the crystallization process. The silica cores can be dissolved in ammonia solution to generate soluble silicate species, which might deposit on the TiO_2 matrix. The formed silica nanocoating might limit the structural reconstruction and prevent the growth of the amorphous TiO_2 species into large crystalline domains. Meanwhile, in neutral condition, silica is very stable and TiO_2/HDA composite layers can be easily transformed into anatase shells.

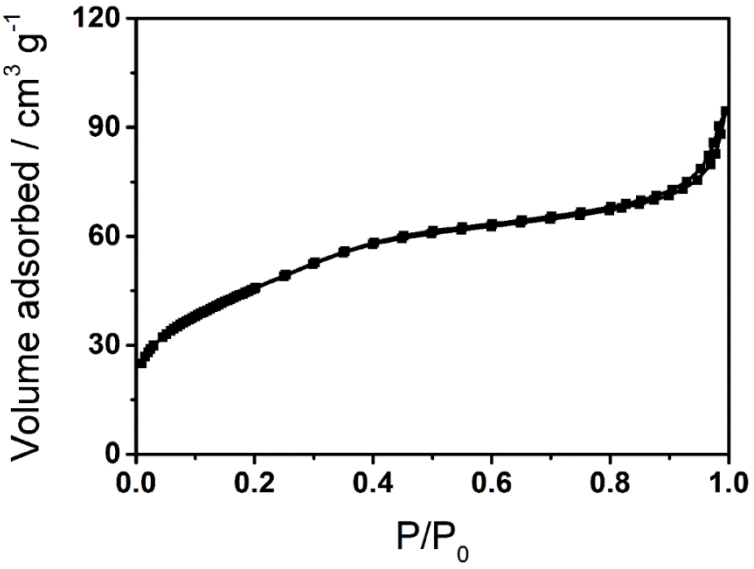

Fig. S14. N_2 sorption analysis of *c*TiO_2 hollow spheres.

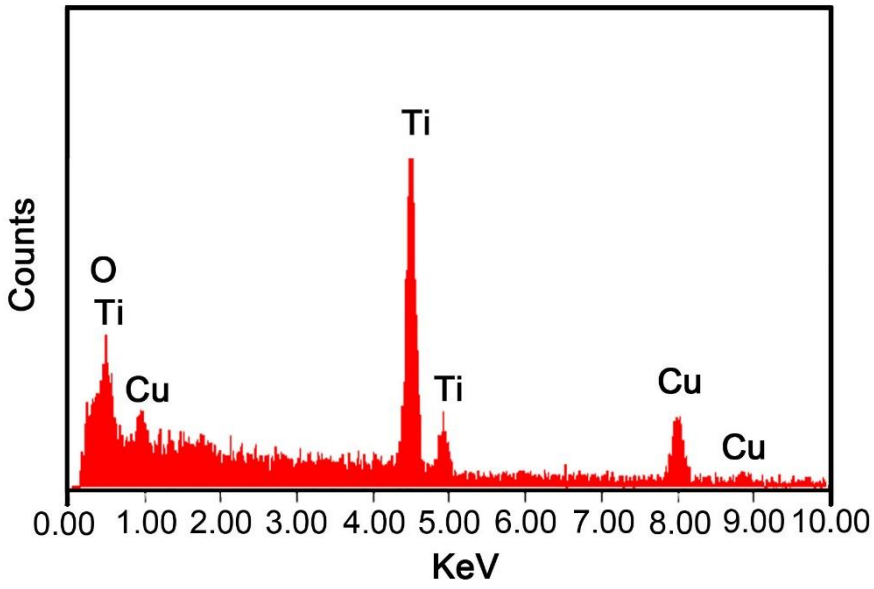

Fig. S15. Elemental analysis. EDX spectrum of *c*TiO_2 hollow spheres.

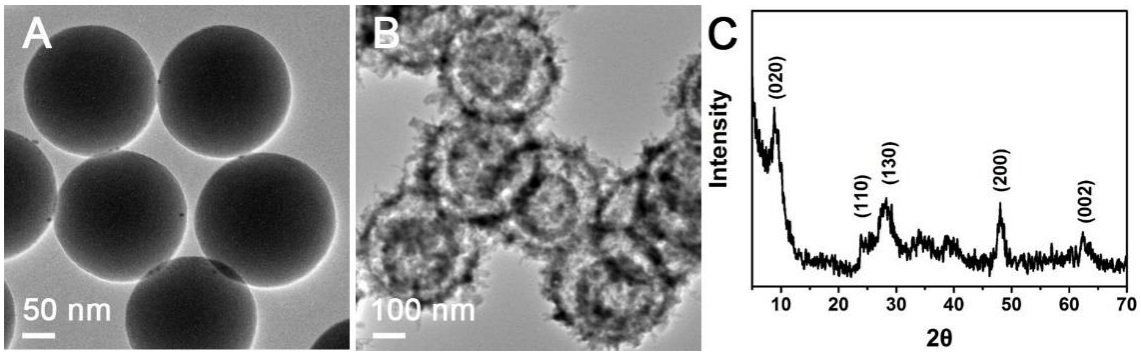

Fig. S16. TEM and XRD characterizations. (**A**) Bare SiO_2 cores obtained after a solvothermal treatment (160 ^oC, 16 h) of the SiO_2@TiO_2/HDA spheres in 0.1 M HCl solution. (**B**) Double-shelled titanate spheres obtained after a solvothermal treatment (160 ^oC, 16 h) of the SiO_2@TiO_2/HDA spheres in 0.1 M NaOH solution, and (**C**) XRD pattern of double-shelled titanate spheres. As can be seen, the pH value has some effect on the morphology and crystallinity of the final products during the solvothermal process. When 0.1 M HCl solution was used, the TiO_2 shells dissolved and only SiO_2 cores remained. The reason may be that the TiO_2/HDA composite shells are unstable in acidic condition. We have successfully prepared double-shelled titanate spheres via a solvothermal treatment of SiO_2@TiO_2/HDA spheres in 0.1 M NaOH solution. The XRD pattern collected from the double-shelled sample can be indexed to an orthorhombic titanate phase.

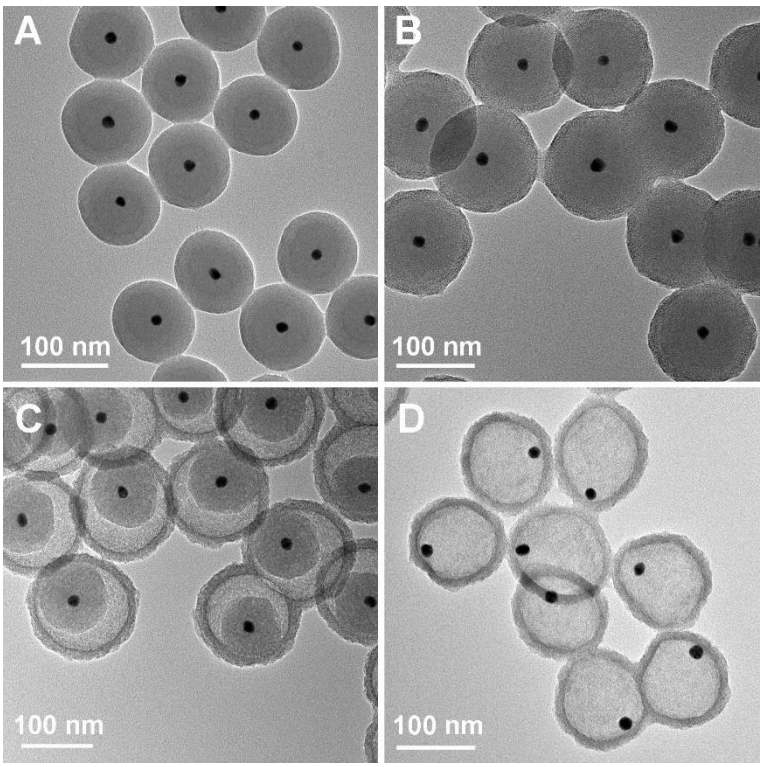

Fig. S17. TEM characterizations of the formation process of Au@TiO_2 yolk-shell spheres. (**A**) Au@SiO_2 core-shell nanospheres, (**B**) Au@SiO_2@TiO_2 core-double-shell nanospheres, (**C**) Au@SiO_2@TiO_2 yolk-shell nanospheres, and (**D**) Au@TiO_2 yolk-shell nanospheres.

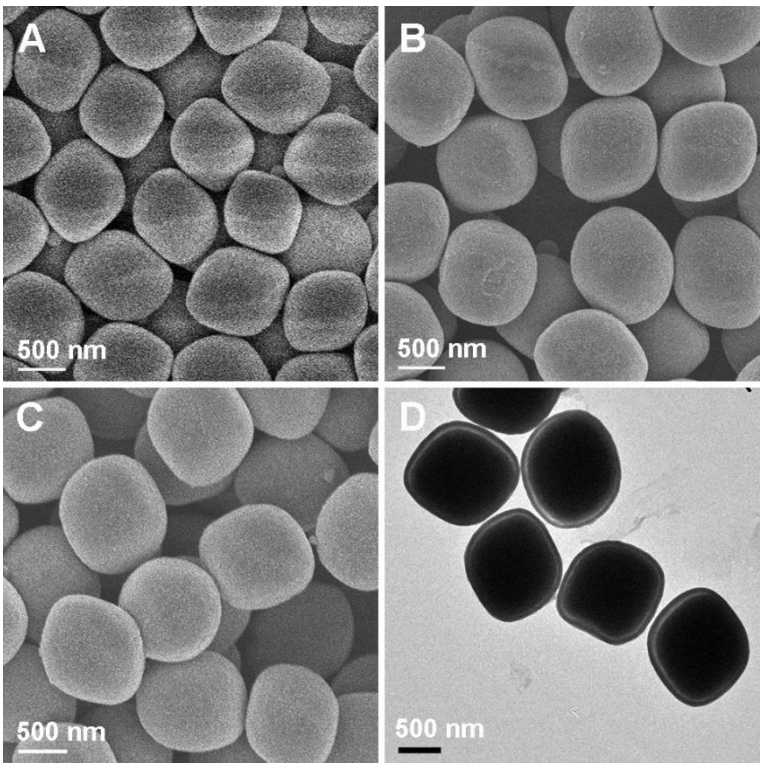

Fig. S18. FESEM and TEM characterizations of the formation process of Fe_2O_3@TiO_2 yolk-shell particles. (**A**) Fe_2O_3@SiO_2 core-shell particles, (**B**) Fe_2O_3@SiO_2@TiO_2 core-double-shell particles, (**C**) Fe_2O_3@TiO_2 yolk-shell particles, and (**D**) Fe_2O_3@TiO_2 yolk-shell particles.

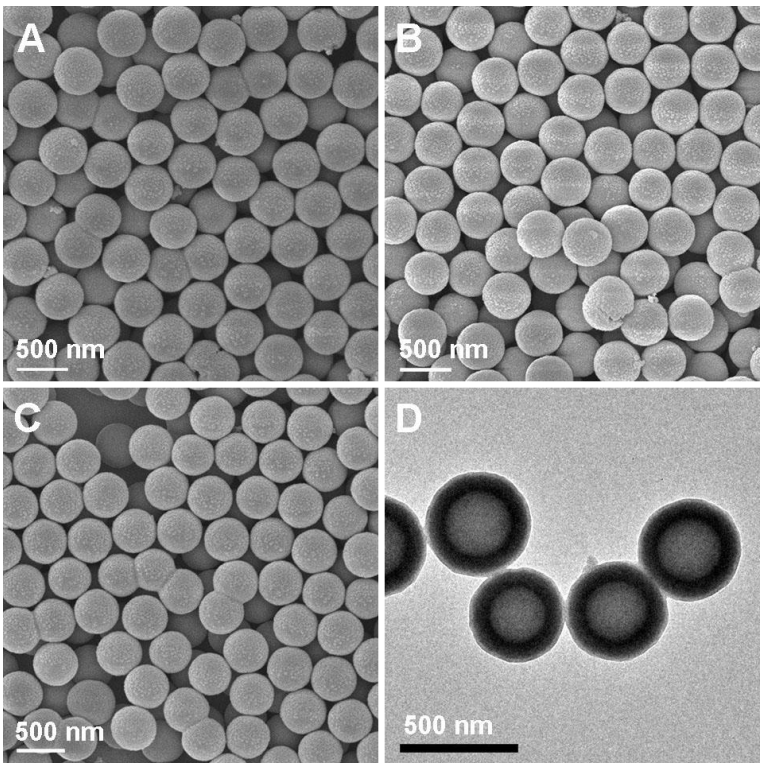

Fig. S19. FESEM and TEM characterizations of the formation process of TiO_2-polymer double-shell hollow spheres. (**A**) SiO_2@TiO_2 core-shell nanospheres, (**B**) TiO_2 hollow spheres, (**C**) TiO_2-polymer double-shell hollow spheres, and (**D**) TiO_2-polymer double-shell hollow spheres.

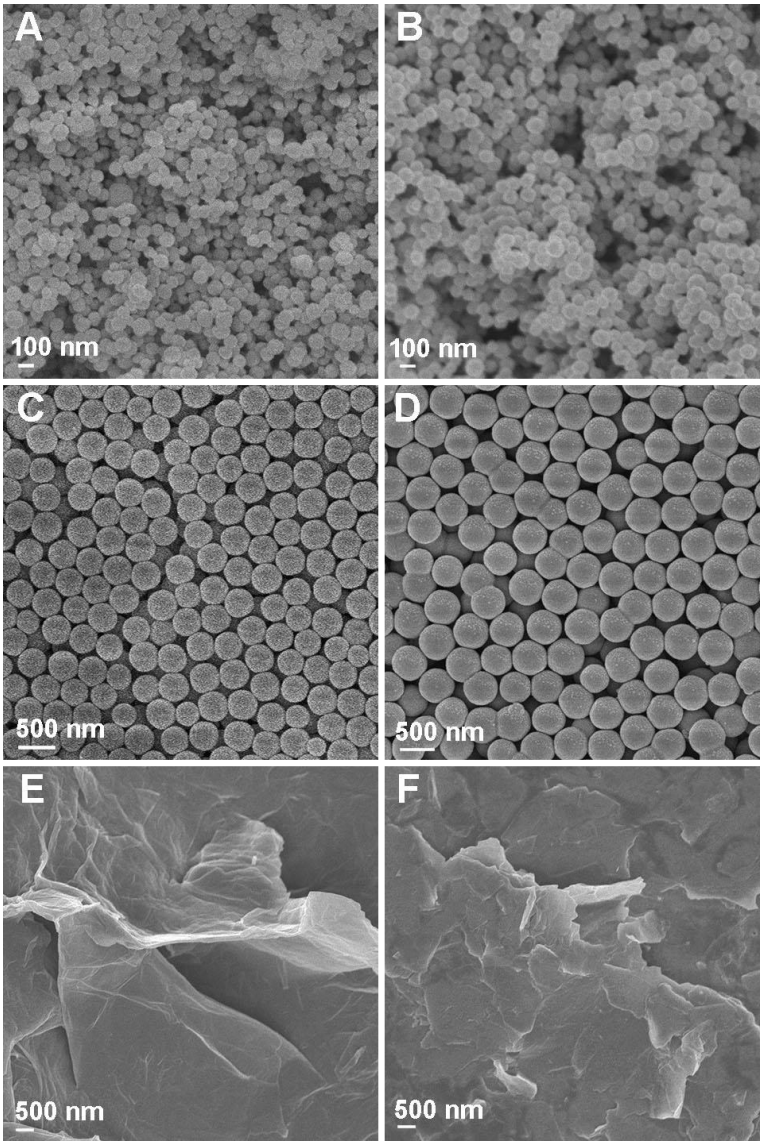

Fig. S20. FESEM characterization of different TiO_2 core-shell composites. (**A**) Mesoporous silica nanospheres (MSNs), (**B**) MSN@TiO_2 core-shell nanospheres, (**C**) polymer nanospheres (PNs), (**D**) PN@TiO_2 core-shell nanospheres, (**E**) graphene oxide (GO) sheets, and (**F**) GO@TiO_2 composite sheets.

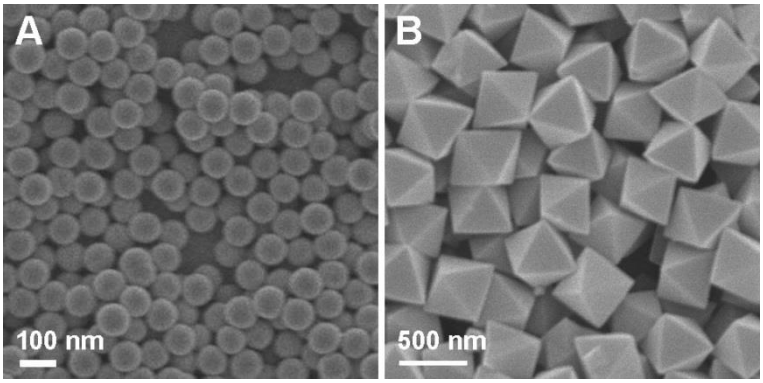

Fig. S21. FESEM characterization of carbon nanosphere and metal-organic framework templates. (**A**) Carbon nanospheres (CNs) and (**B**) metal-organic framework (MOF) crystals.

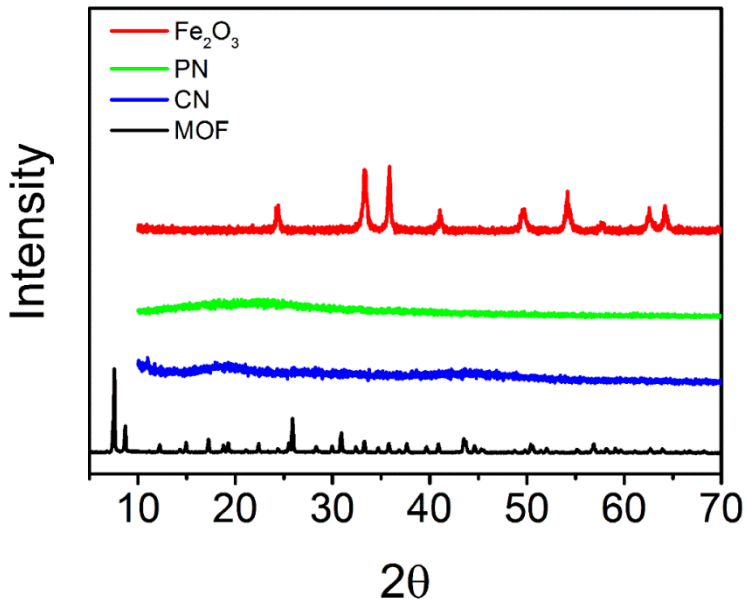

Fig. S22. Wide-angle XRD analysis of different functional cores. XRD patterns of Fe_2O_3, PN, CN, and MOF cores. All the identified peaks in the XRD patterns of Fe_2O_3 and MOF can be ascribed to *α*-Fe_2O_3 and UiO-66 without noticeable signals of any impurities. The wide-angle XRD patterns of PN and CN confirm the amorphous nature of these nanospheres.

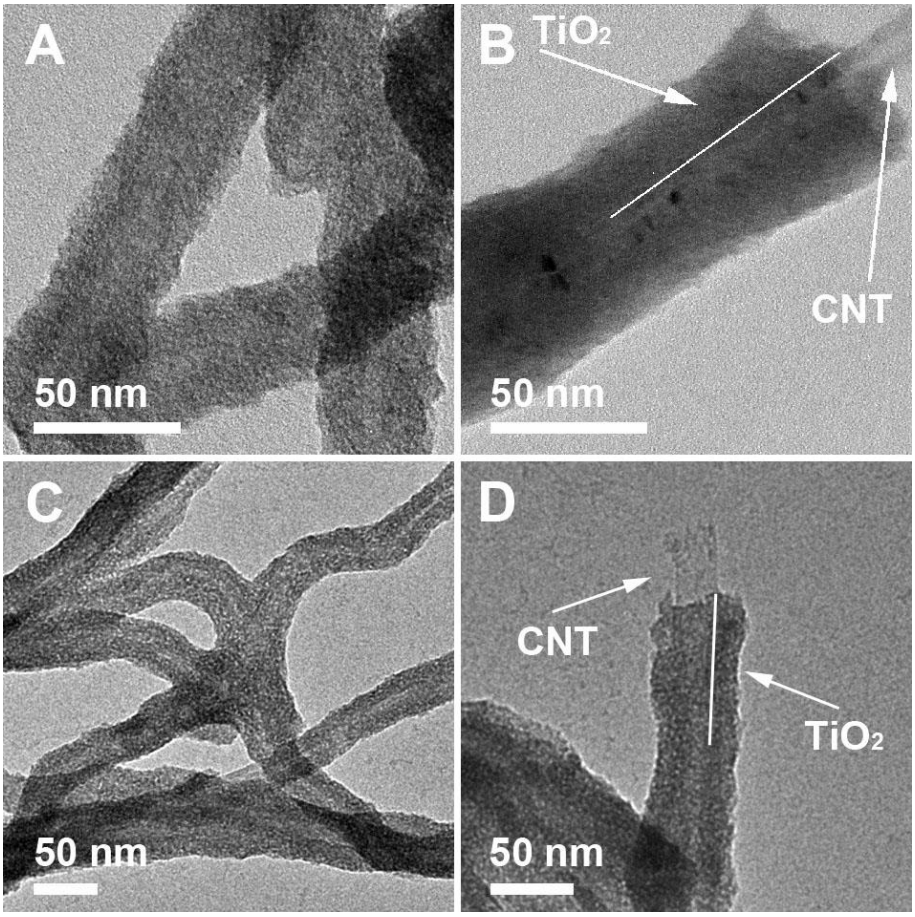

Fig. S23. TEM characterization of carbon nanotube@TiO_2 nanofibers. (**A** and **B**) carbon nanotube (CNT, treated with HNO_3) @TiO_2 core-shell nanofibers. (**C** and **D**) untreated carbon nanotube@TiO_2 core-shell nanofibers. In a typical synthesis, 8 mg of treated or untreated CNTs (Bought from Timesnano Company, China) was homogeneously dispersed in ethanol (9.74 mL) by ultrasonication, followed by the addition of 0.08 g of hexadecylamine (HDA, 90%) and 0.2 mL of ammonia (25% - 28%) and then stirred at room temperature for 1 min to form uniform dispersion. Then, 0.15 mL of titanium isopropoxide (TIP) was added to the dispersion under stirring. After stirring for 10 min, the CNT@TiO_2 nanofibers were collected by centrifugation then washed with water and ethanol several times.

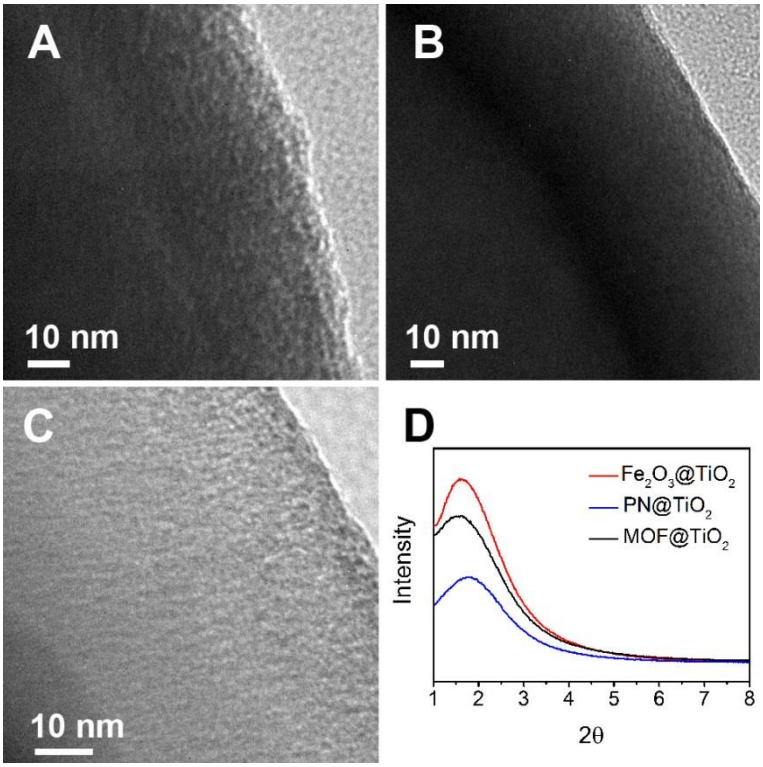

Fig. S24. TEM characterization and small-angle XRD analysis of different TiO_2 core-shell composites. Magnified TEM images of (**A**) Fe_2O_3@TiO_2 yolk-shell cubes, (**B**) PN@TiO_2 core-shell particles, and (**C**) MOF@TiO_2 core-shell particles. (**D**) Their small-angle XRD patterns.

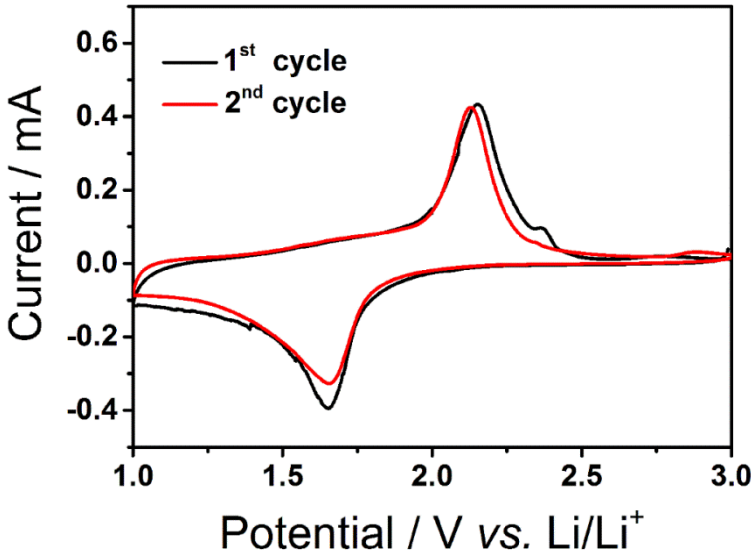

Fig. S25. Cyclic voltammograms of *c*TiO_2 hollow spheres in the voltage window of 1.0-3.0 V *vs.* Li/Li^+ at a scan rate of 0.2 mV s^{-1}.

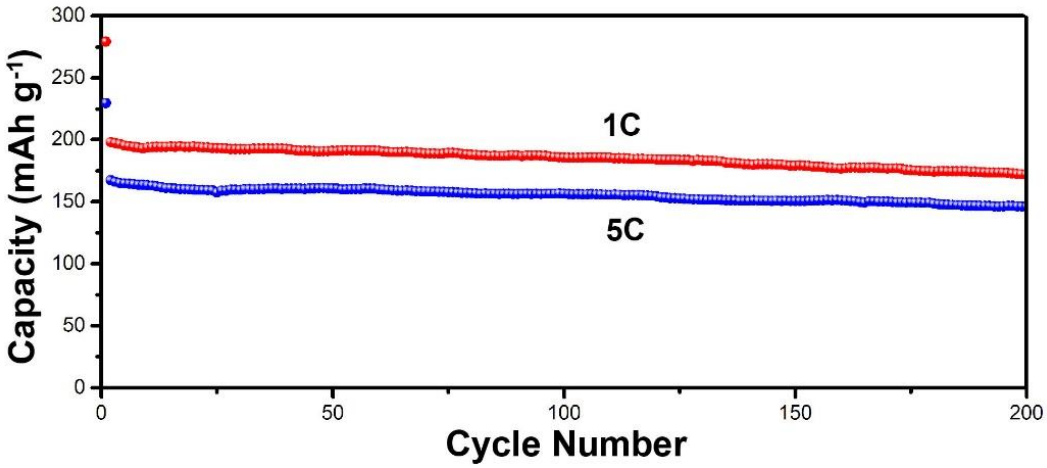

Fig. S26. Electrochemical characterization of *c*TiO_2 hollow spheres as an anode material in LIBs. Cycling performance of *c*TiO_2 hollow spheres at current densities of 1 C and 5 C. 1 C=173 mA g^{-1}.

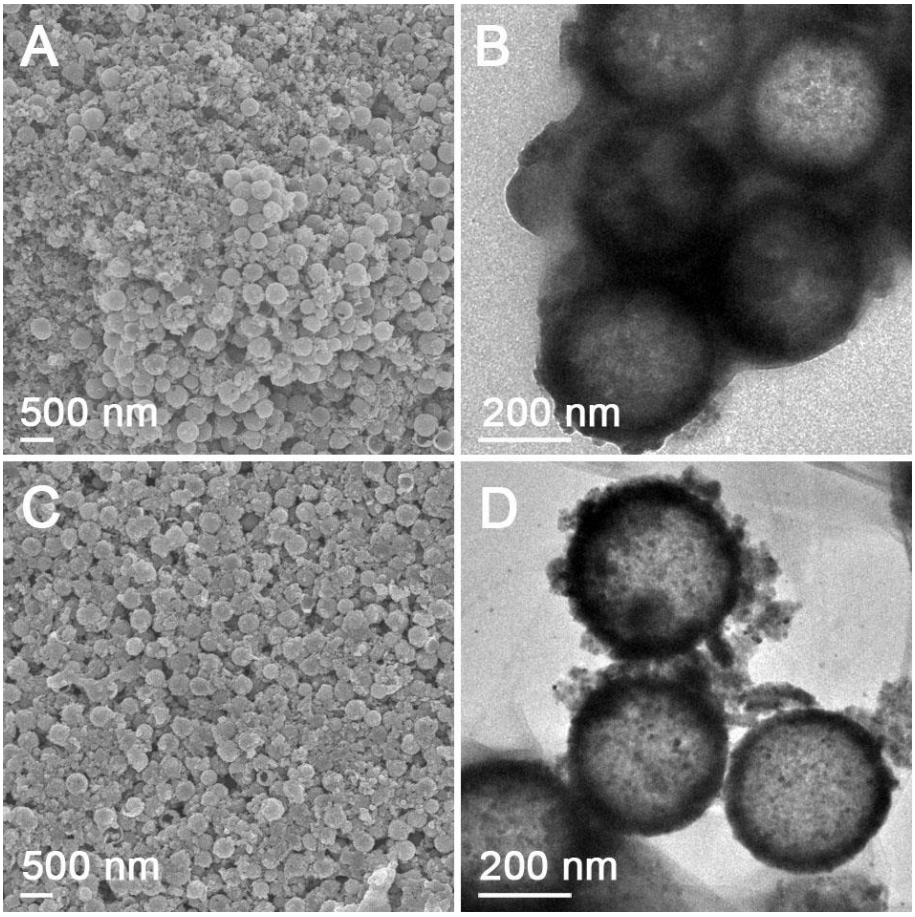

Fig. S27. FESEM and TEM images of *c*TiO_2 hollow spheres before and after cycling test. (**A and B**) before cycling, and (**C and D**) after cycling for 100 cycles.